Transmission Electron Microscope (TEM) Imaging Basics

Cindy Smith

References:
Electron Microscopy of Thin Crystals, Hirsch et. al.
Transmission Electron Microscopy and Diffractometry of Materials, B. Fultz & J. M. Howe
Transmission Electron Microscopy, Williams & Carter

In-situ Equipment

JEOL 4000 Controlled Environment Transmission Electron Microscope

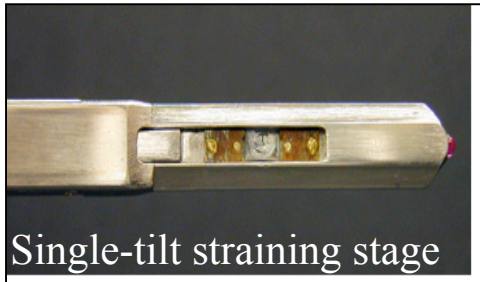

Single-tilt straining stage

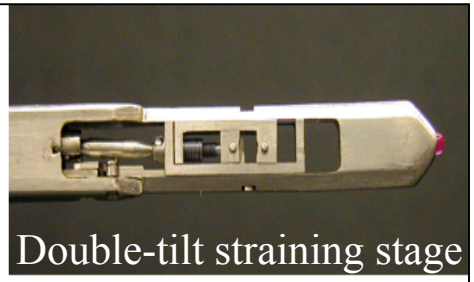

Double-tilt straining stage

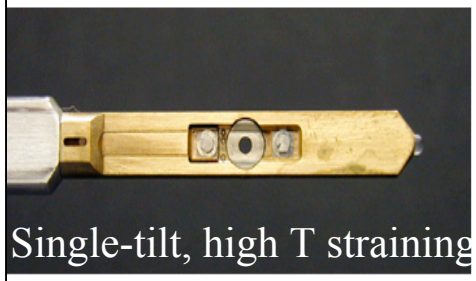

Single-tilt, high T straining

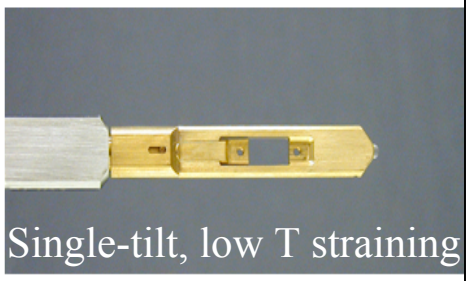

Single-tilt, low T straining

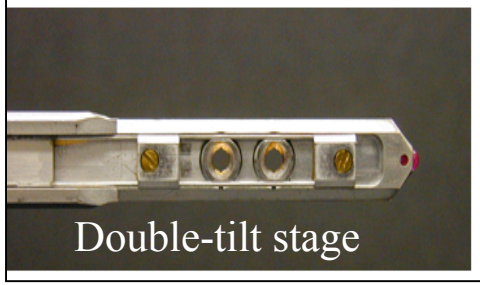

Double-tilt stage

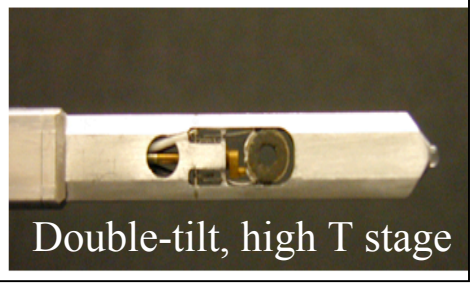

Double-tilt, high T stage

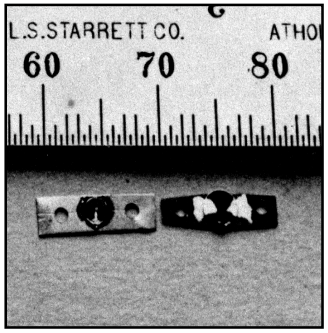

Sample stages and sample geometries

D. K. Dewald, T. C. Lee, J. A. Eades, I. M. Robertson and H. K. Birnbaum Review of Scientific Instruments, 62, 1438, 1991.

Interaction of High Energy Electrons with a Sample

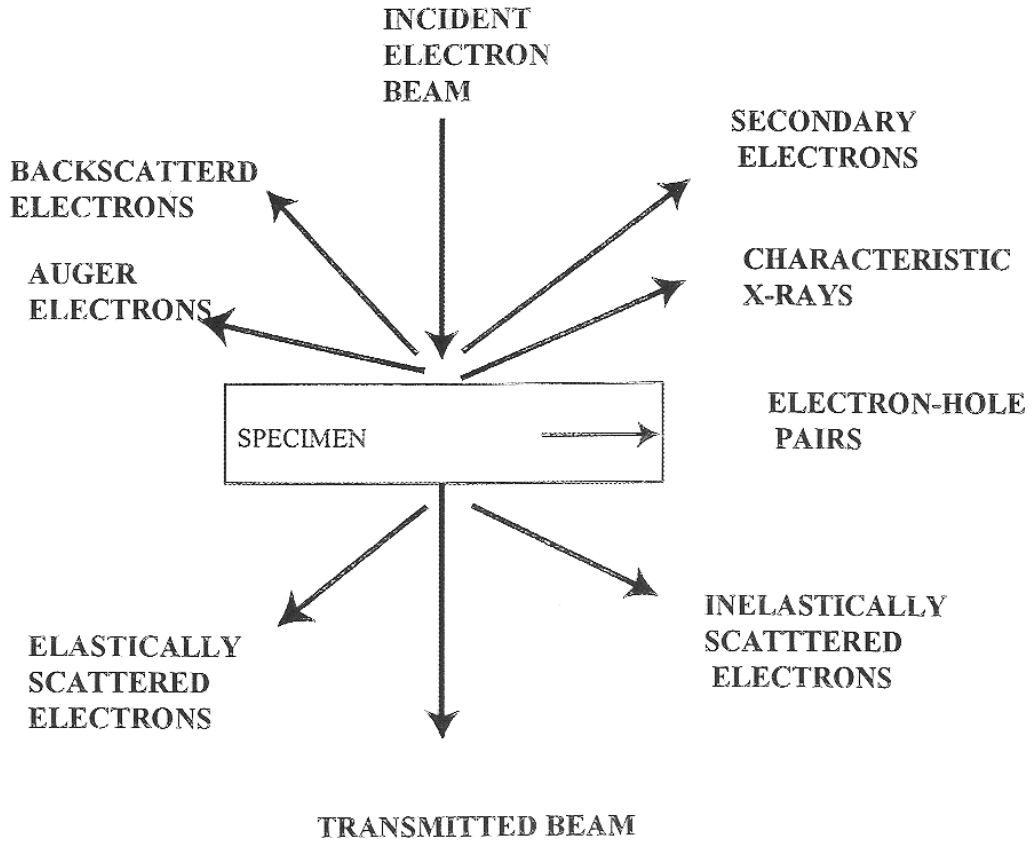

Bragg's law

$$n\lambda = 2\,d\sin\theta_B$$

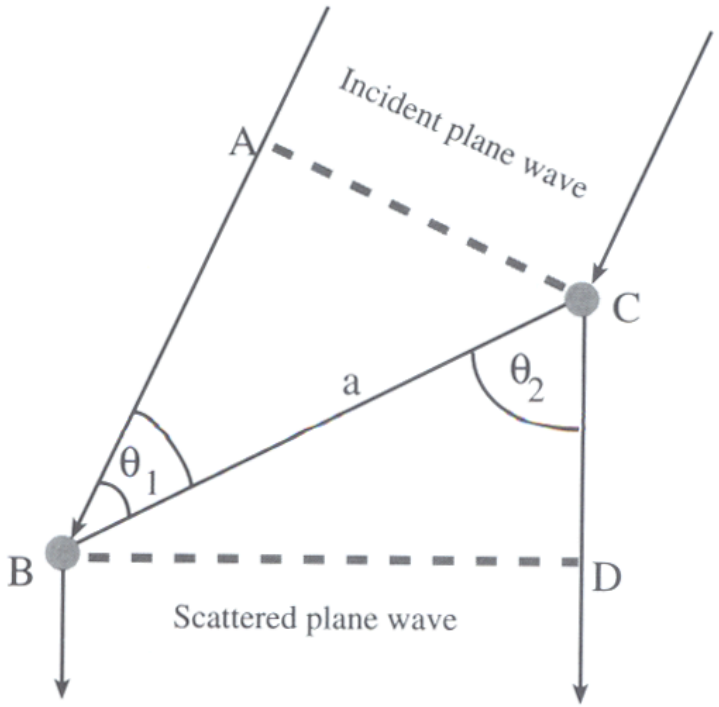

Figure 3.8. The approach used by von Laue to calculate the path difference for a wave (wavelength λ). In this one-dimensional figure the wave is incident at angle θ_1 and scattered at angle θ_2 from two atoms (B and C) spaced distance *a* apart. The path difference between scattered waves is AB – CD.

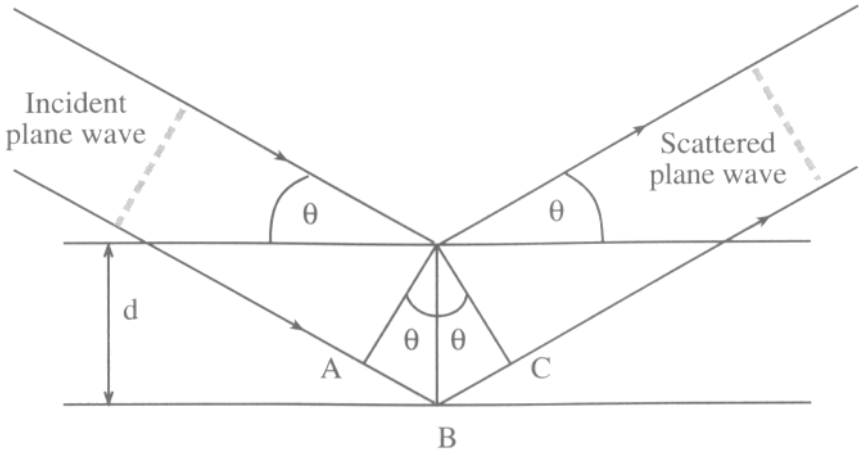

Figure 3.9. The Bragg description of diffraction in terms of the reflection of a plane wave (wavelength λ) incident at an angle θ to atomic planes of spacing *d*. The path difference between reflected waves is AB + BC.

Lens-Ray Diagram of TEM

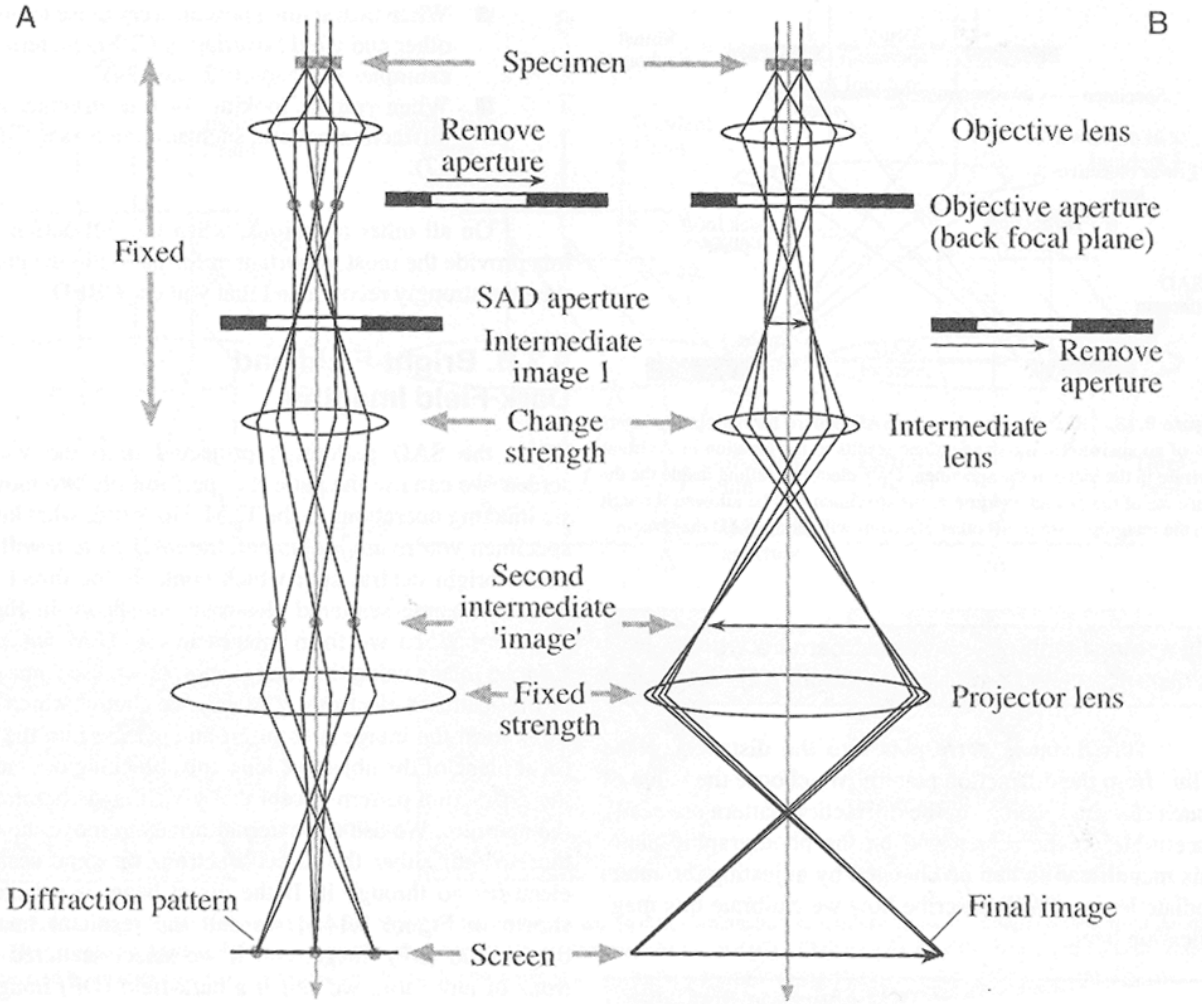

Diffraction Pattern Image

Image formation in the TEM
Bright Field (BF)

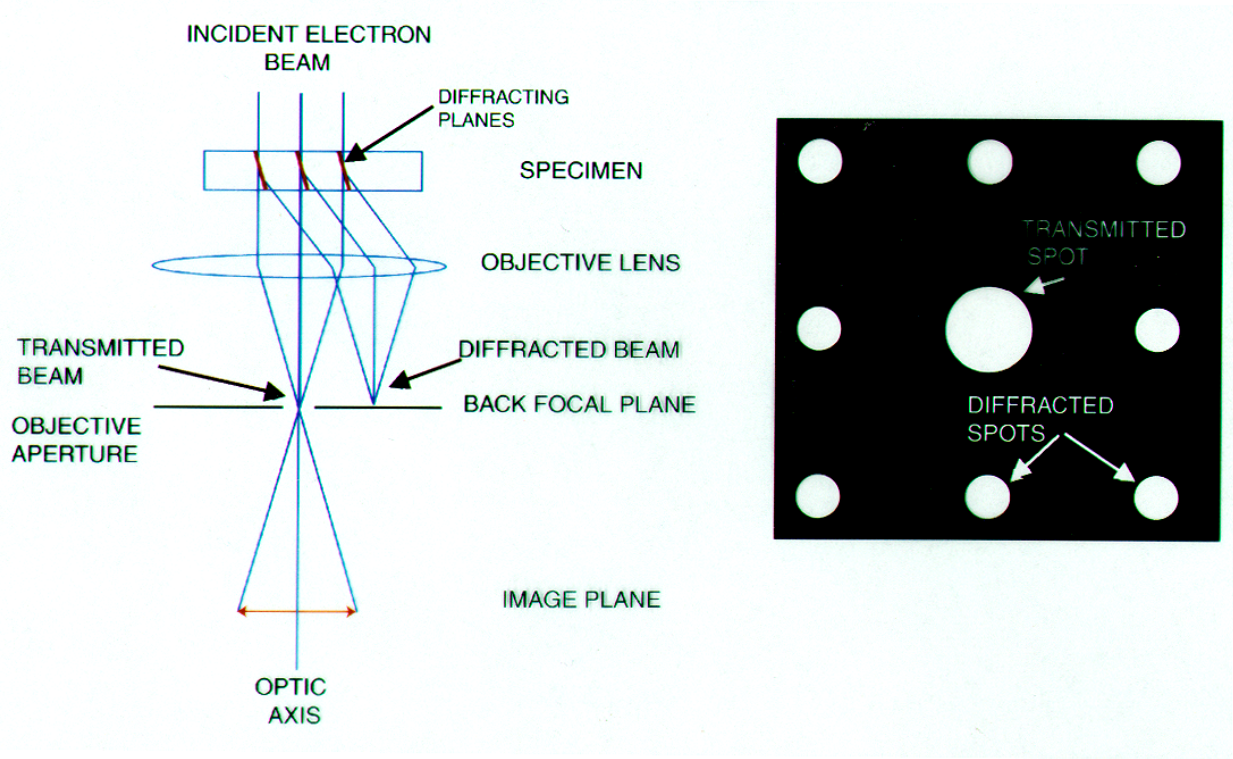

Image formation in the TEM
Dark Field (DF)

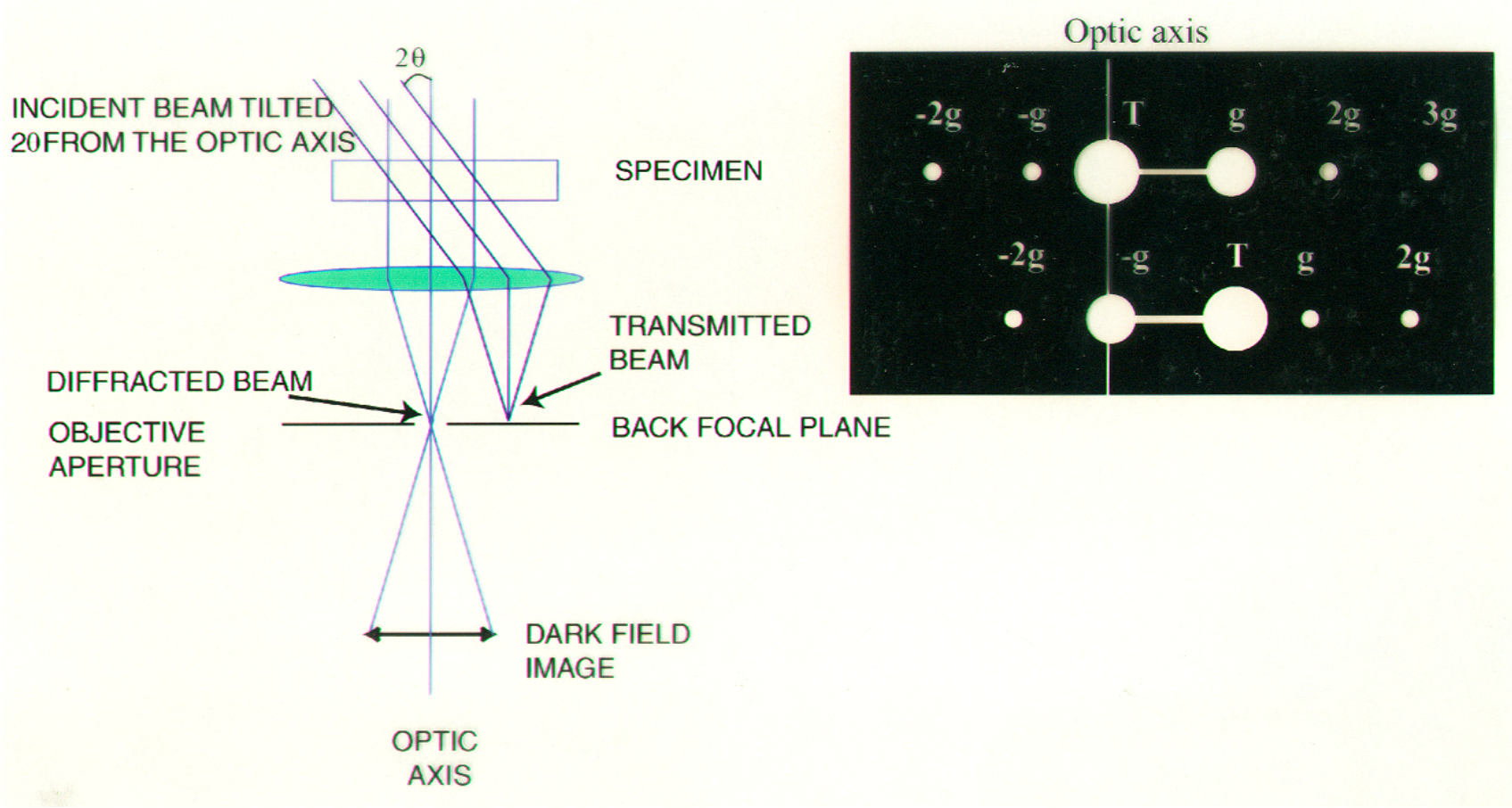

TEM images of Au islands on C film, BF & DF

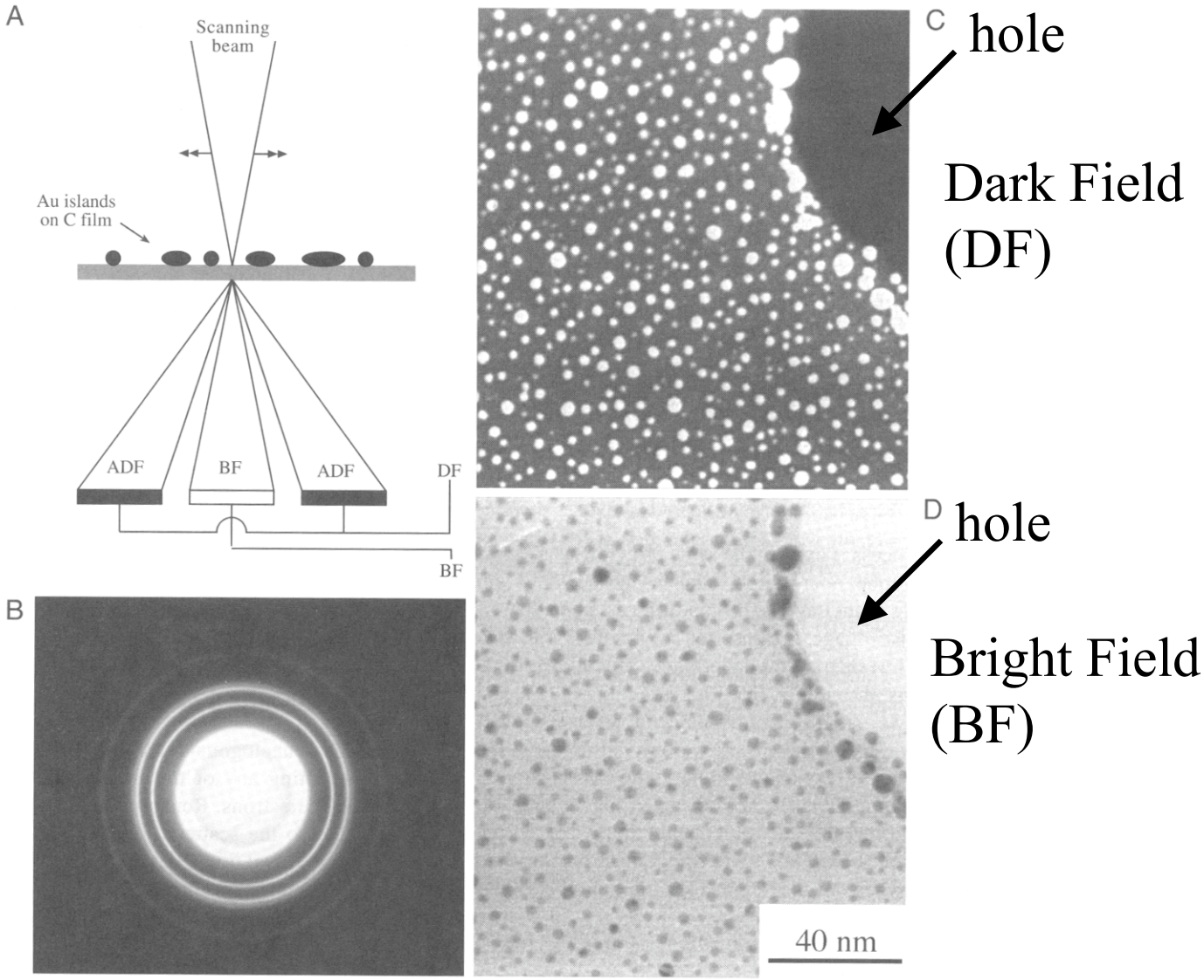

Figure 9.18. STEM image formation: A BF detector is placed in a conjugate plane to the back focal plane to intercept the direct beam (A) and a concentric annular DF detector intercepts the diffracted electrons (B). The signals from either detector are amplified and modulate the STEM CRT. The specimen (Au islands on a C film) gives complementary ADF (C) and BF (D) images.

Location of dislocation image related to dislocation core

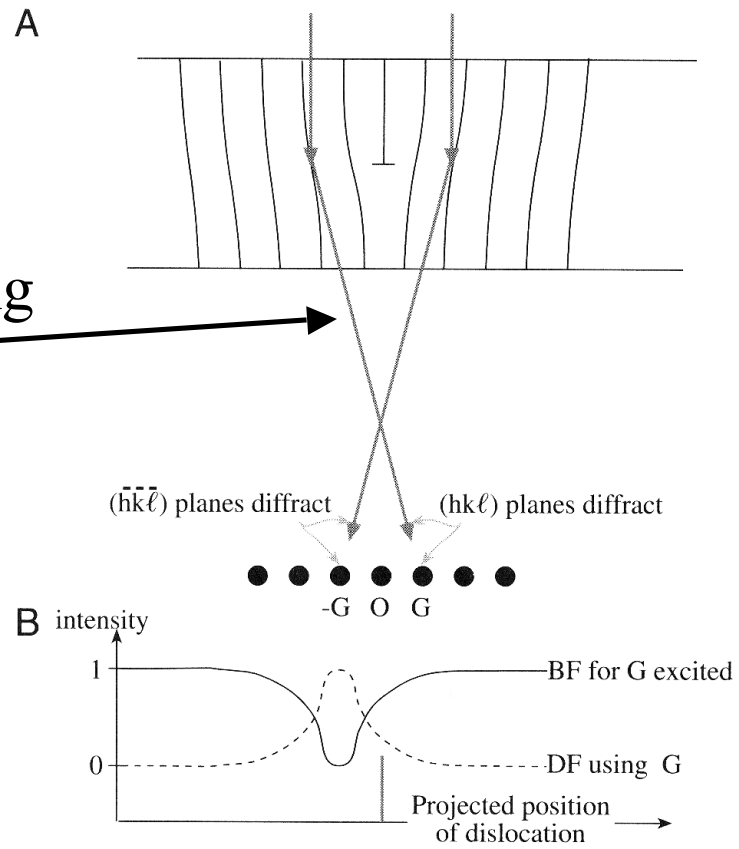

Figure 25.1. (A) The specimen is tilted slightly away from the Bragg condition ($\mathbf{s} \neq 0$). The distorted planes close to the edge dislocation are bent back into the Bragg-diffracting condition ($\mathbf{s} = 0$), diffracting into G and –G as shown. (B) Schematic profiles across the dislocation image showing that the defect contrast is displaced from the projected position of the defect.

Location of dislocation image related to dislocation core

Diagram showing dislocation image lying to one side of the dislocation core

- **The dislocation image is located between 4 and 10 nm from the dislocation core.**
- **The dislocation image width is between 4 and 10 nm.**

Equation describing the change in amplitude of the diffracted wave as it travels through a crystal containing a defect

$$\frac{d\phi_g}{dz} = \frac{\pi i}{\xi_g}\phi_o + 2\pi i s_{eff}\phi_g$$

$$s_{eff} = s + \underline{g} \bullet \frac{d\underline{R}}{dz}$$

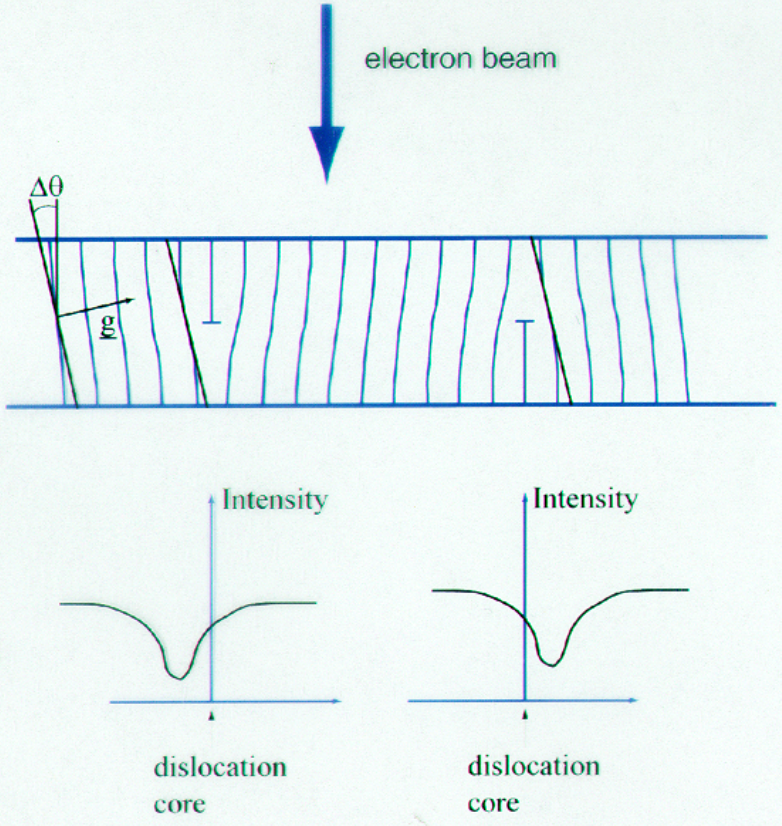

Two-beam diffraction conditions (used in g • b analysis of dislocations)

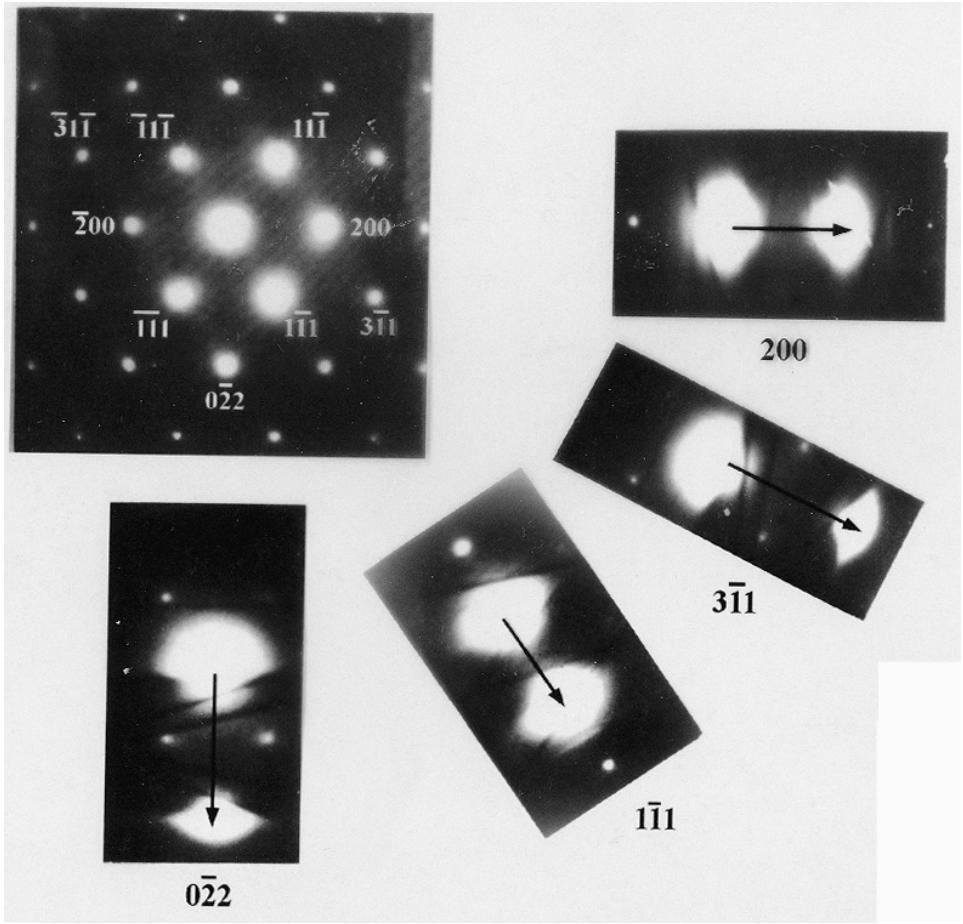

Images of Dislocations due to diffraction conditions

Single image
Two beam BF

Double image
Three beam BF

Transmitted
Diffracted

Transmitted
Diffracted

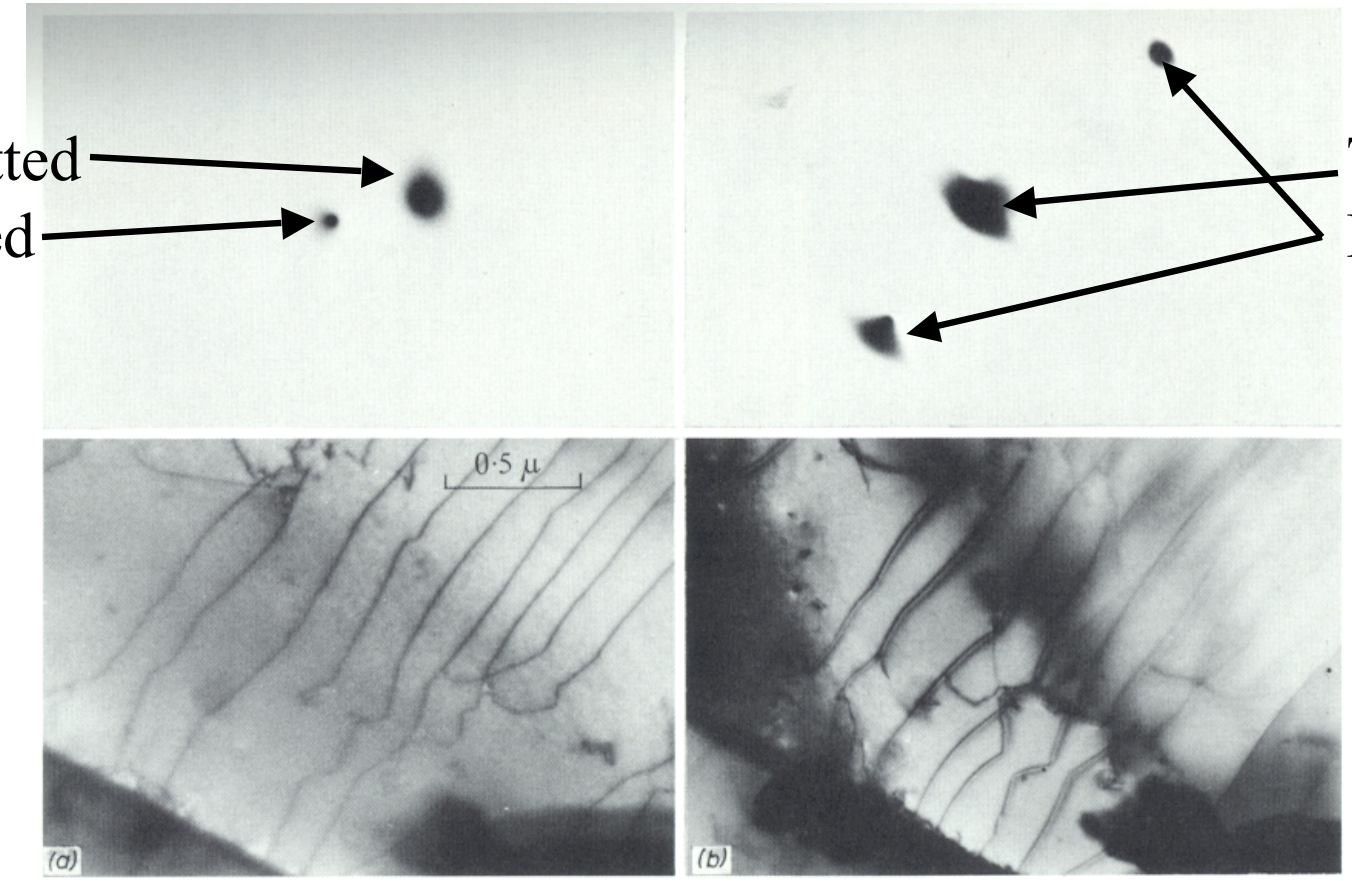

Figure 7.26. Double images of dislocations in nickel: (a) single images when one reflection is operating; (b) double images when two reflections are operating. The associated diffraction patterns are also shown
(From Hirsch, Howie and Whelan, 1960, by courtesy of The Royal Society)

Weak-beam (WB or WBDF) image formation

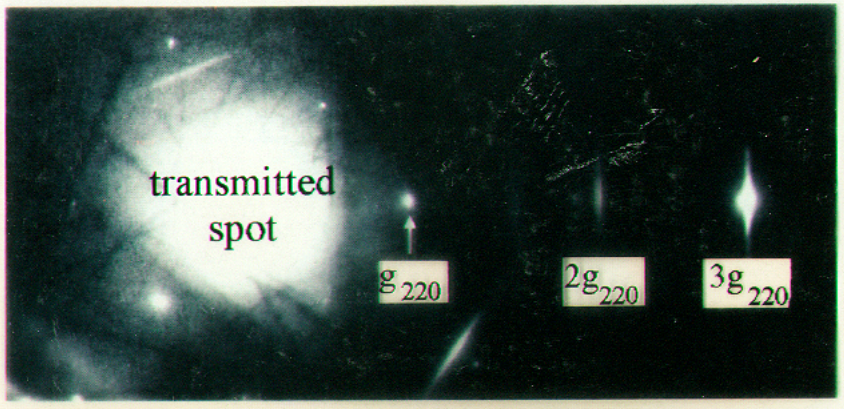

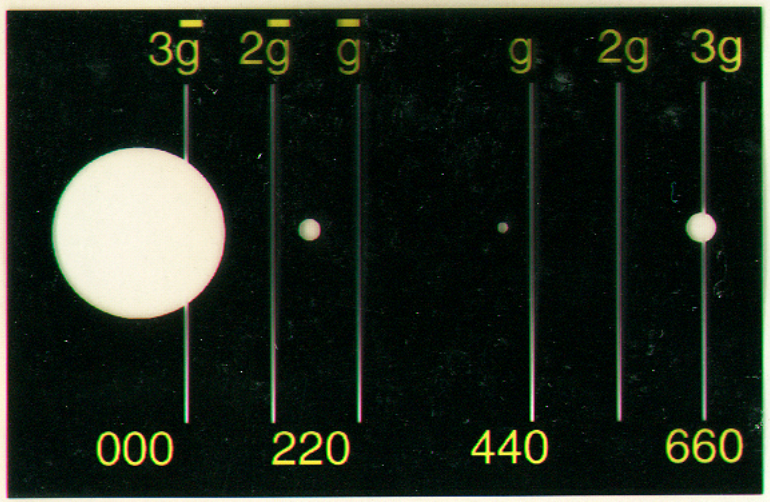

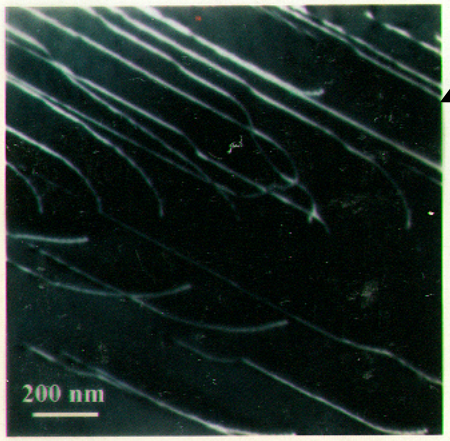

Dislocations are white

- **Sample is tilted so that 3g is excited.**
- **Deviation from Bragg (s_g) is large(between 2-3 x 10^{-2} $Å^{-1}$).**
- **Image from region where planes are severely bent, close to dislocation core.**
- **Image width is between 1 and 2 nm and the image is located between 1and 2 nm from the core**
- **Objective aperture surrounds g_{220} to form the image**

Weak-beam dark field (WBDF) dislocation images

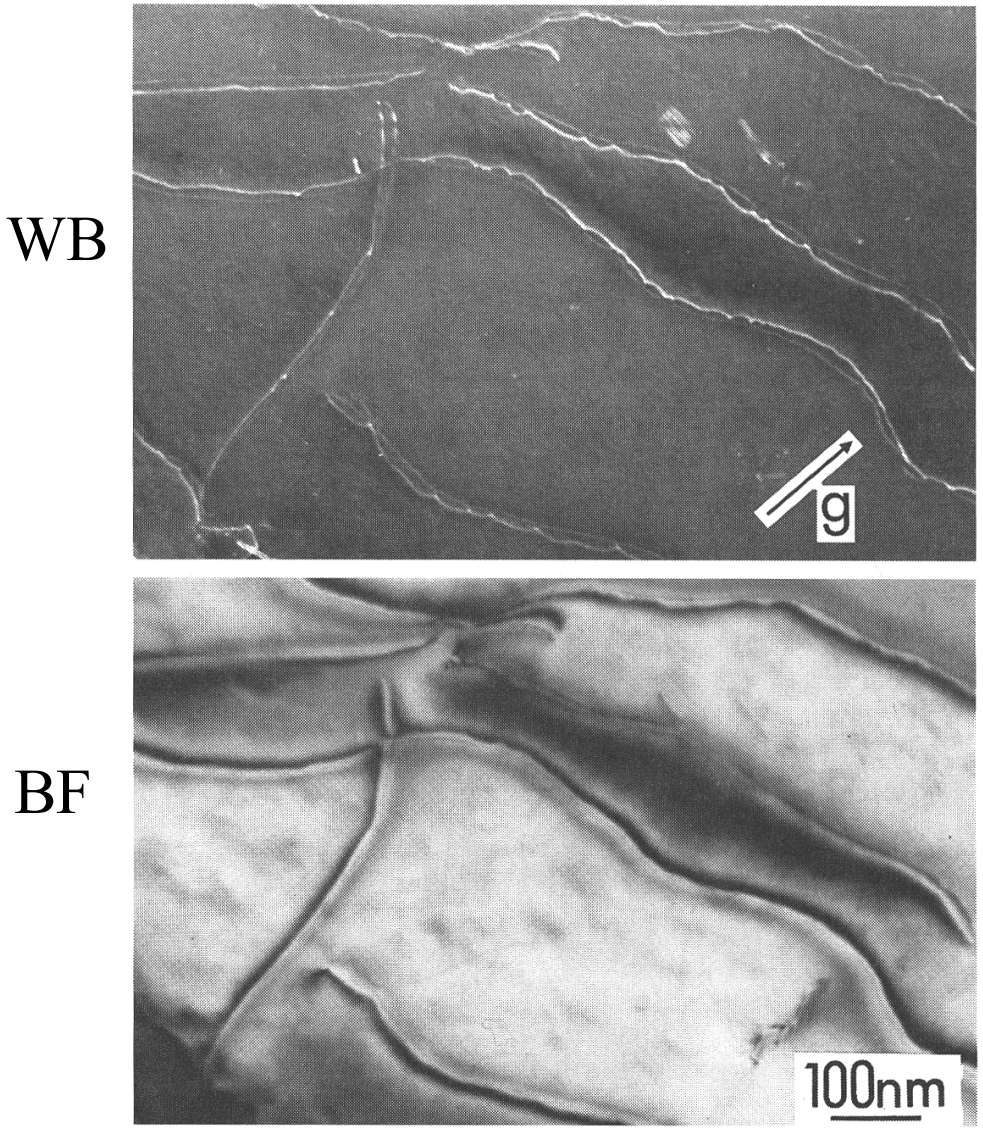

Figure 26.8. A comparison of dislocation images in a Cu alloy formed using (A) WB and (B) strong-beam ($s_g > 0$) conditions.

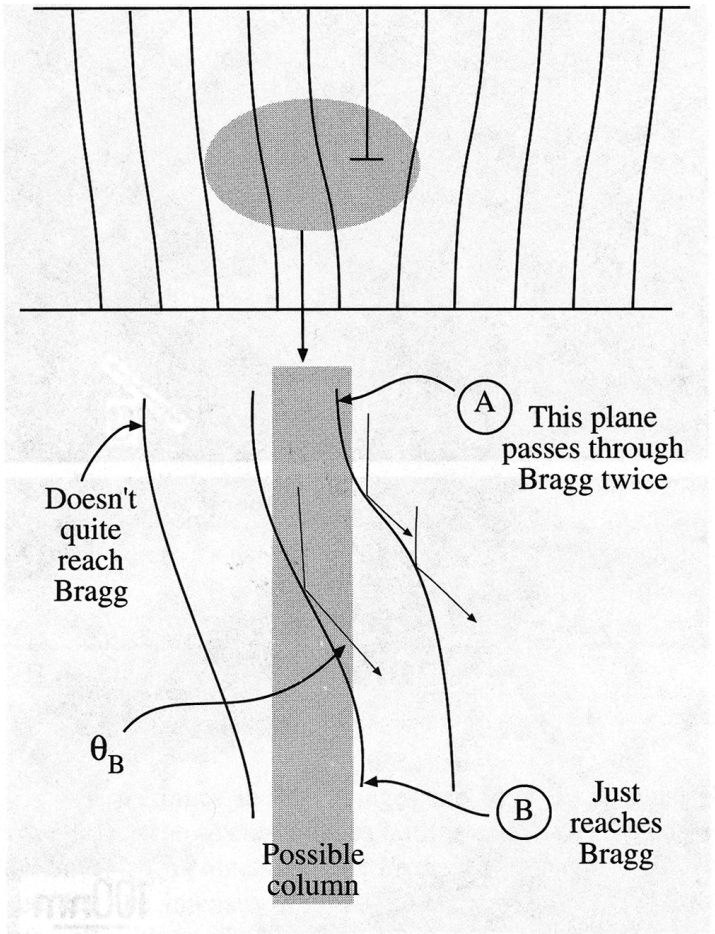

Figure 26.9. WB images of defects show high intensity close to the defect because only there are the diffracting planes bent back into the Bragg condition. This illustration is for an edge dislocation.

Weak-beam dark field (WBDF) dislocation images

Two beam BF WBDF

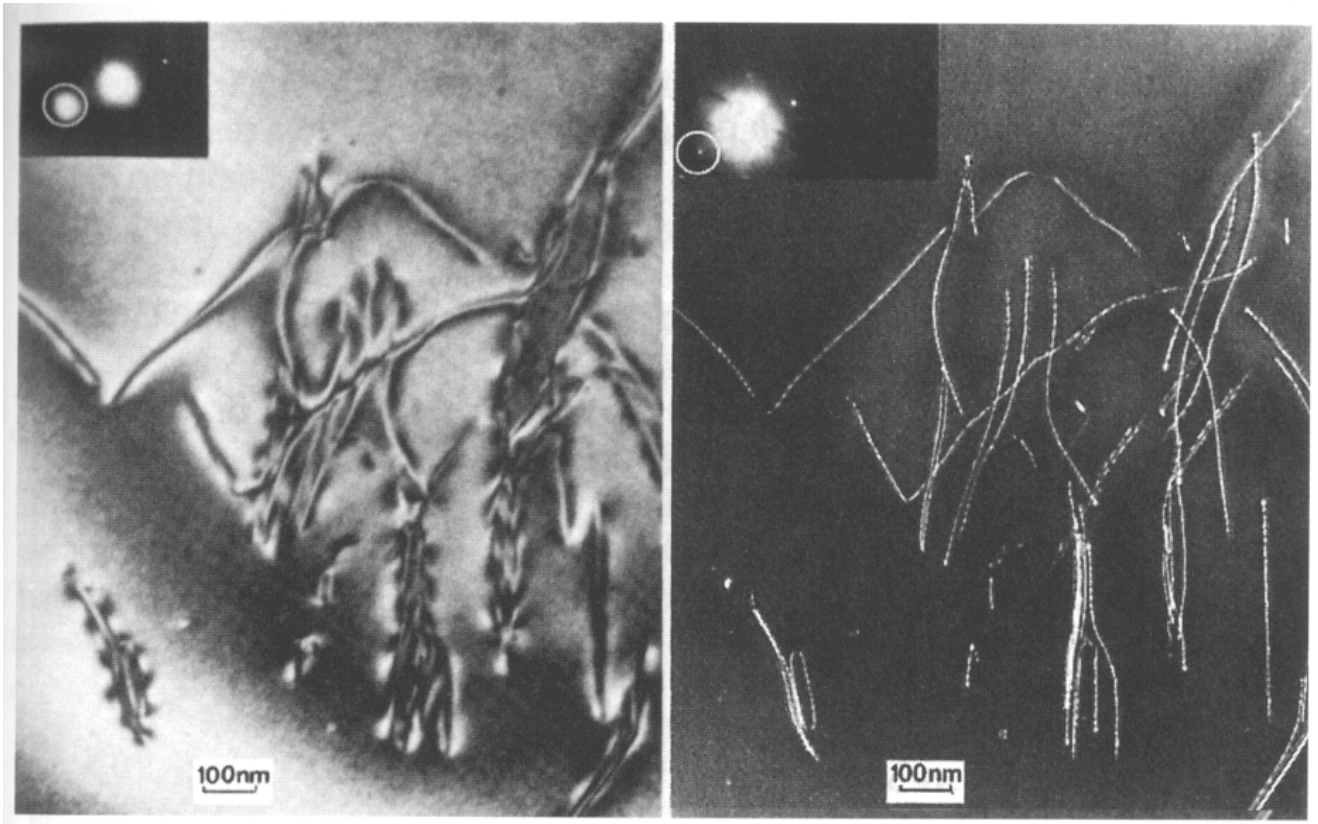

Fig. 7.41. Dislocations in Si. Left: BF image in two-beam condition with strong $(2\bar{2}0)$ diffraction. Right: $\boldsymbol{g}$-$3\boldsymbol{g}$ WBDF image with weak $(2\bar{2}0)$ diffraction. Compare the intensities of the active diffractions (circled in inserts). After [7.9].

Weak-beam dark field (WBDF) dislocation images

Two beam BF

WBDF

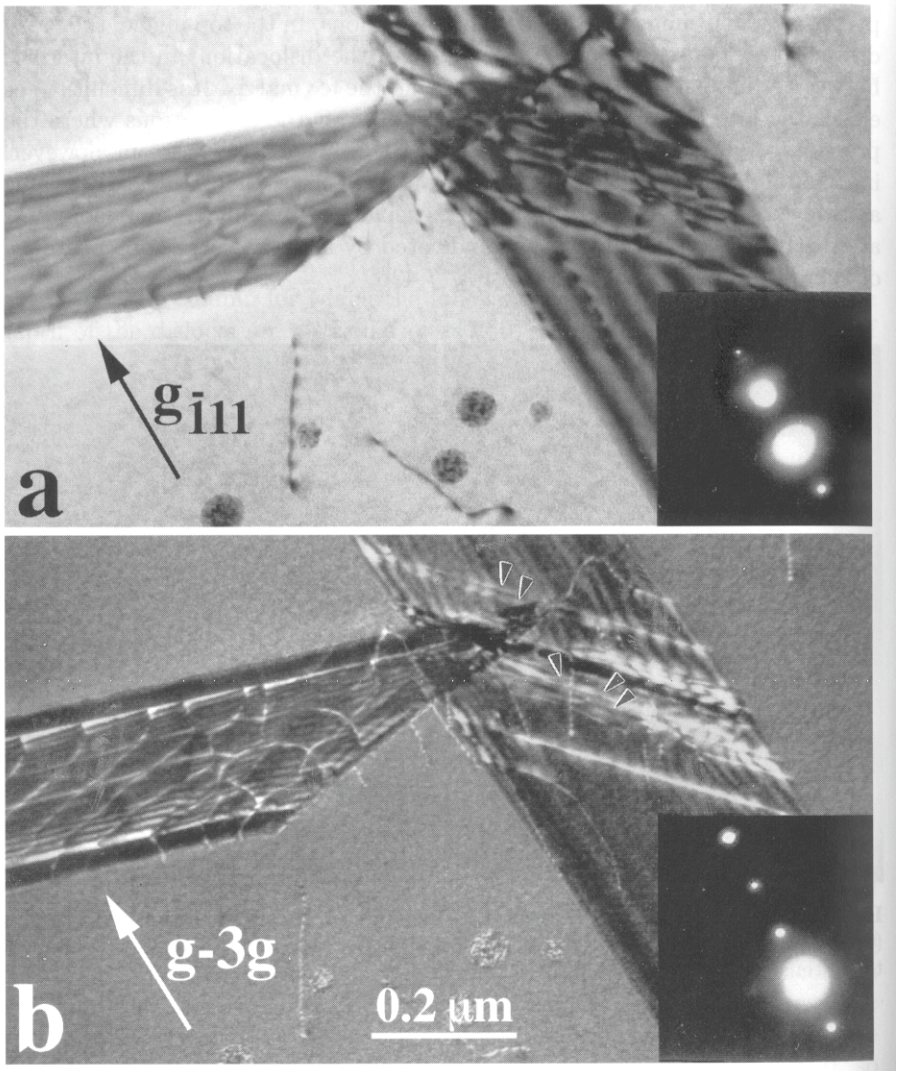

Fig. 7.42. Ag_2Al hcp precipitates in fcc Al-rich matrix in an Al-Ag alloy. (**a**) BF image with strong $(\bar{1}11)$ diffraction. (**b**) ***g*-3*g*** WBDF image with $(\bar{1}11)$ diffraction. The $(\bar{1}11)$ diffraction is the spot just above the forward (brightest) beam in the inserts [7.6].

Kikuchi Diffraction

Specimen must be thick enough to generate a large number of incoherently scattered electrons (diffusely scattered electrons in all directions), which are then Bragg diffracted by the planes.

The beam which was initially closest to the optic axis, and therefore more intense, is further away after being scattered. This gives the excess line and the deficient line.

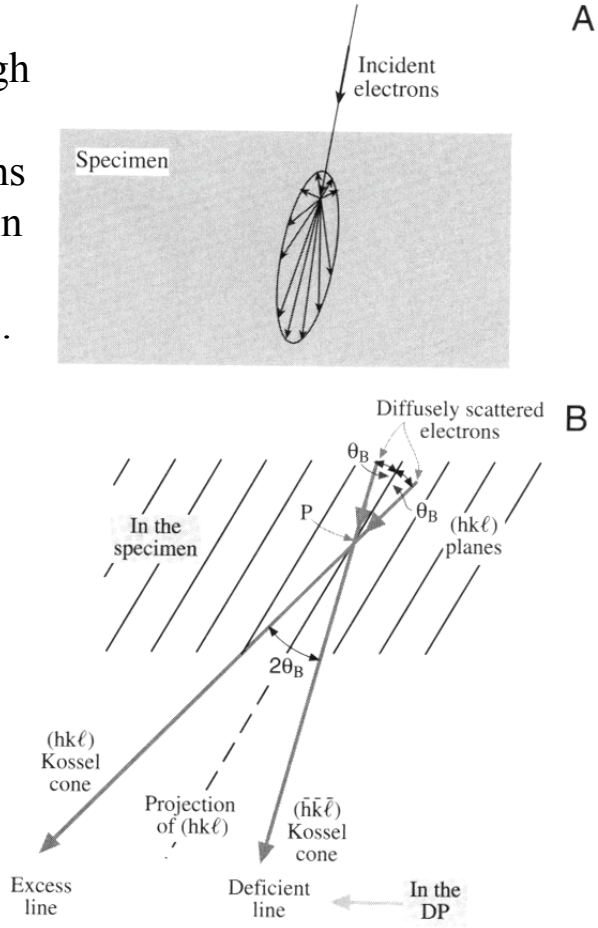

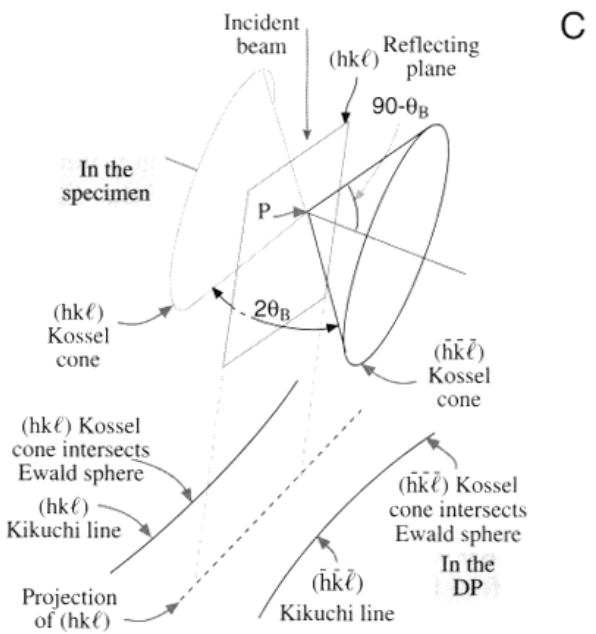

Figure 19.2. (A) Schematic representation of all electron scattering localized at a single point in the specimen. In (B) some of the scattered electrons are diffracted because they travel at the Bragg angles θ_B to certain $hk\ell$ planes. The diffracted electrons form Kossel cones centered at P on the diffracting planes. The lines closest to the incident beam direction are dark (deficient) and the lines furthest away from the beam are bright (excess). In (C) the cones intercept the Ewald sphere, creating parabolas which approximate to straight Kikuchi lines in the diffraction patterns because θ_B is small.

The distance between the **–g** and **g** Kikuchi lines is **g** (not 2**g**) because the angle between the two Kossel cones is $2\theta_B$.

Kikuchi Diffraction

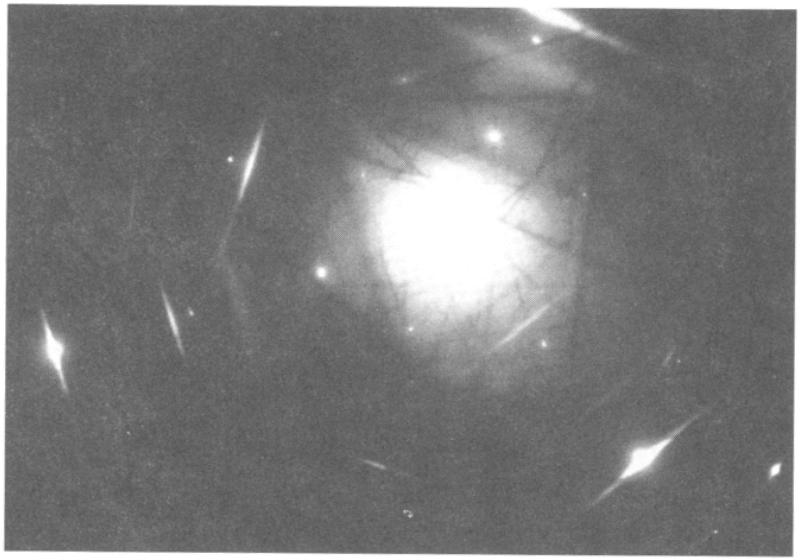

Figure 19.1. An ideal diffraction pattern containing both well-defined spots and clearly visible pairs of bright and dark Kikuchi lines.

When the **g** Kikuchi line passes through the reflection G, then s_g=0 (the Bragg condition is satisfied), and the **–g** Kikuchi line passes through O.
If the direct beam is exactly parallel to the plane *hkl*, the **g** and **–g** Kikuchi lines are symmetrically displaced about O with **g** "passing through" **g**/2 and **–g** "passing through" **–g**/2.

Kikuchi Maps

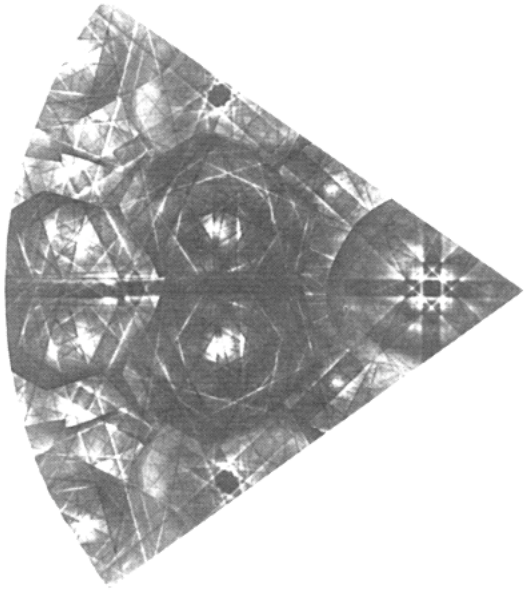

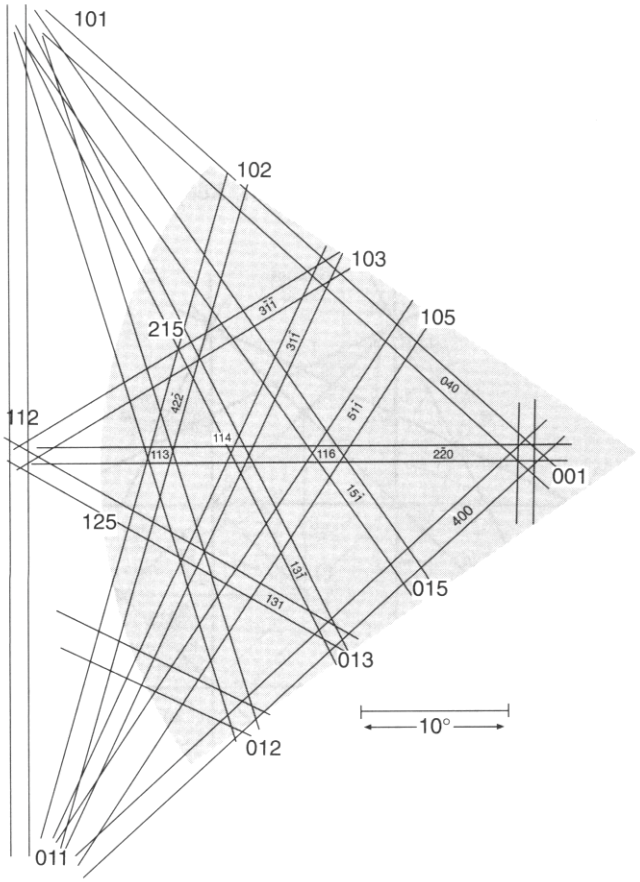

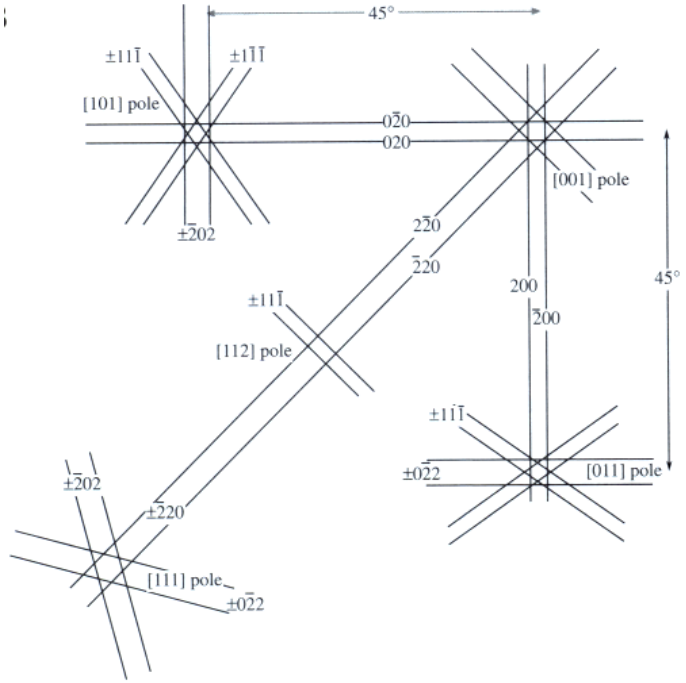

Burgers Vectors

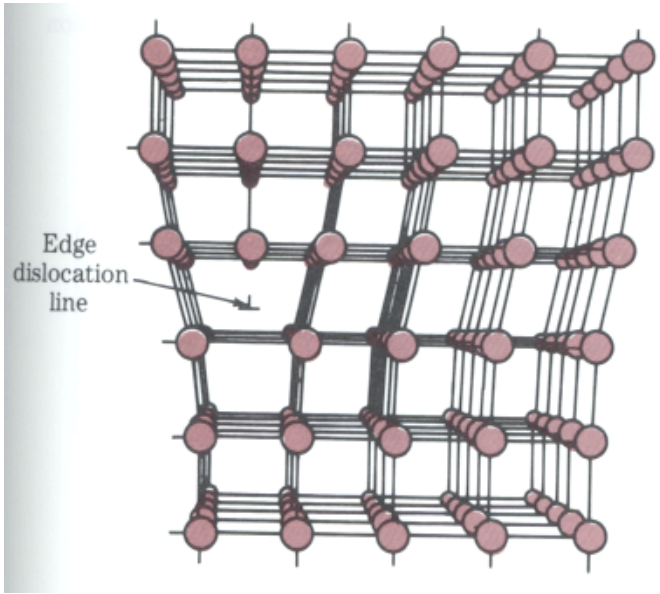

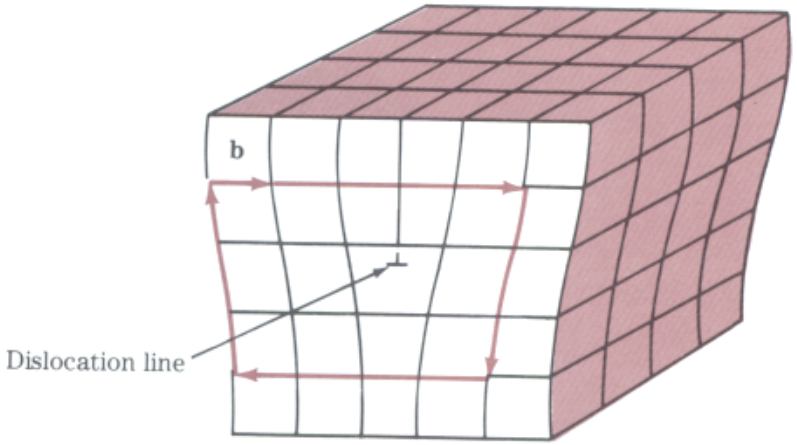

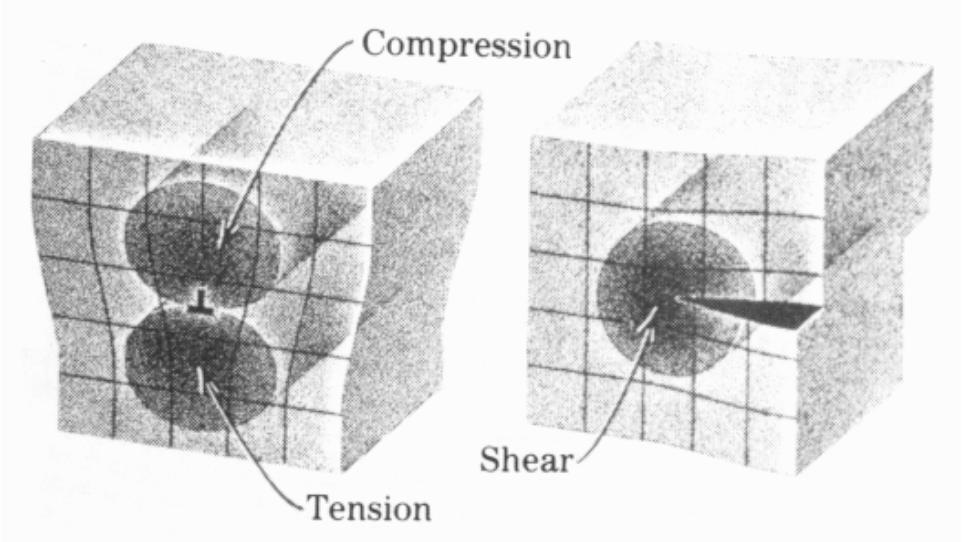

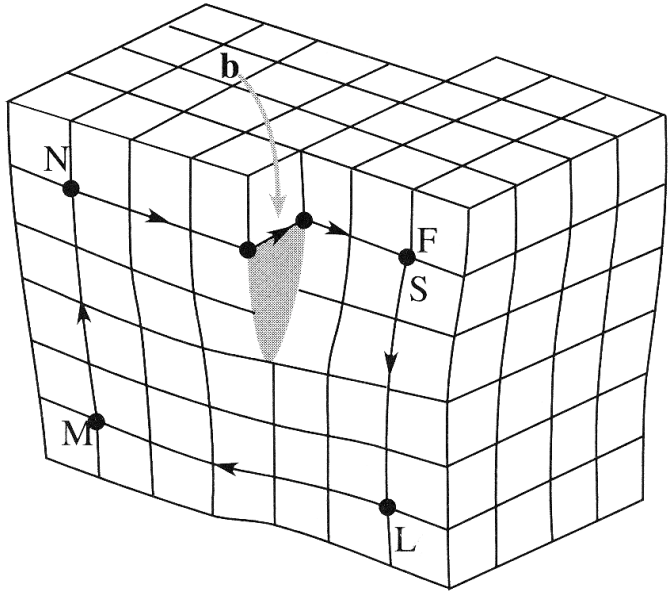

Determining the burgers vector – the g • b rule

Demonstration of the g • b rule

- **Only the planes belonging to g_1 are affected by the presence of the dislocation. Applying g • b gives**

- $g_1 \bullet b \neq 0$
- $g_2 \bullet b = 0$
- $g_3 \bullet b = 0$

  $\therefore \quad g_2 \otimes g_3 = b$

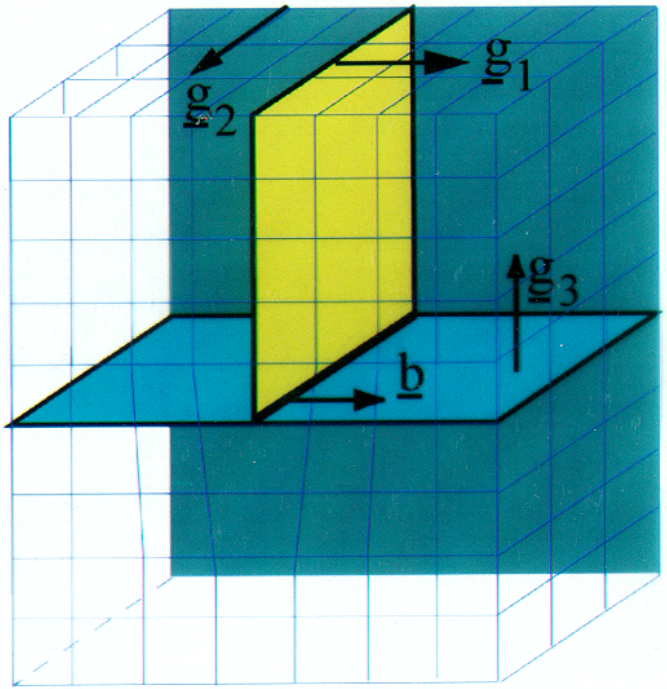

Determining the burgers vector – the g • b rule

Technically, the g • b = 0 criterion is really g • b x u = 0

With g = diffraction vector

b = the burgers vector

u = line direction

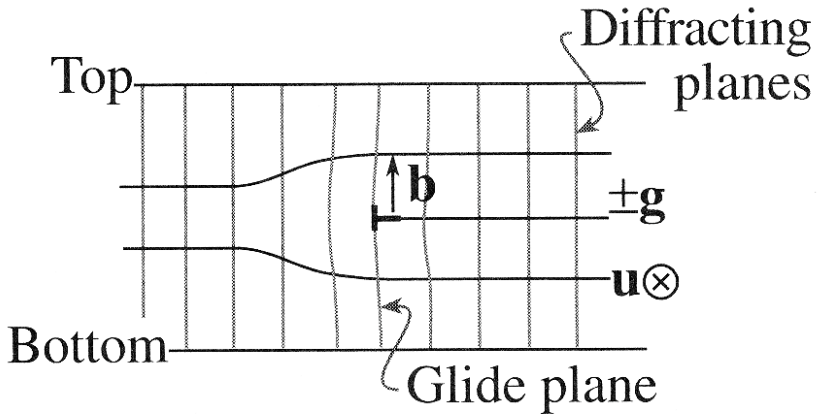

Figure 25.4. Buckling of the glide planes arises because of the term **g**·**b**×**u** and is important because it complicates the analysis of **b**.

Images of Dislocations for different g • b conditions

Single image
Two beam BF

Double image
Three beam BF

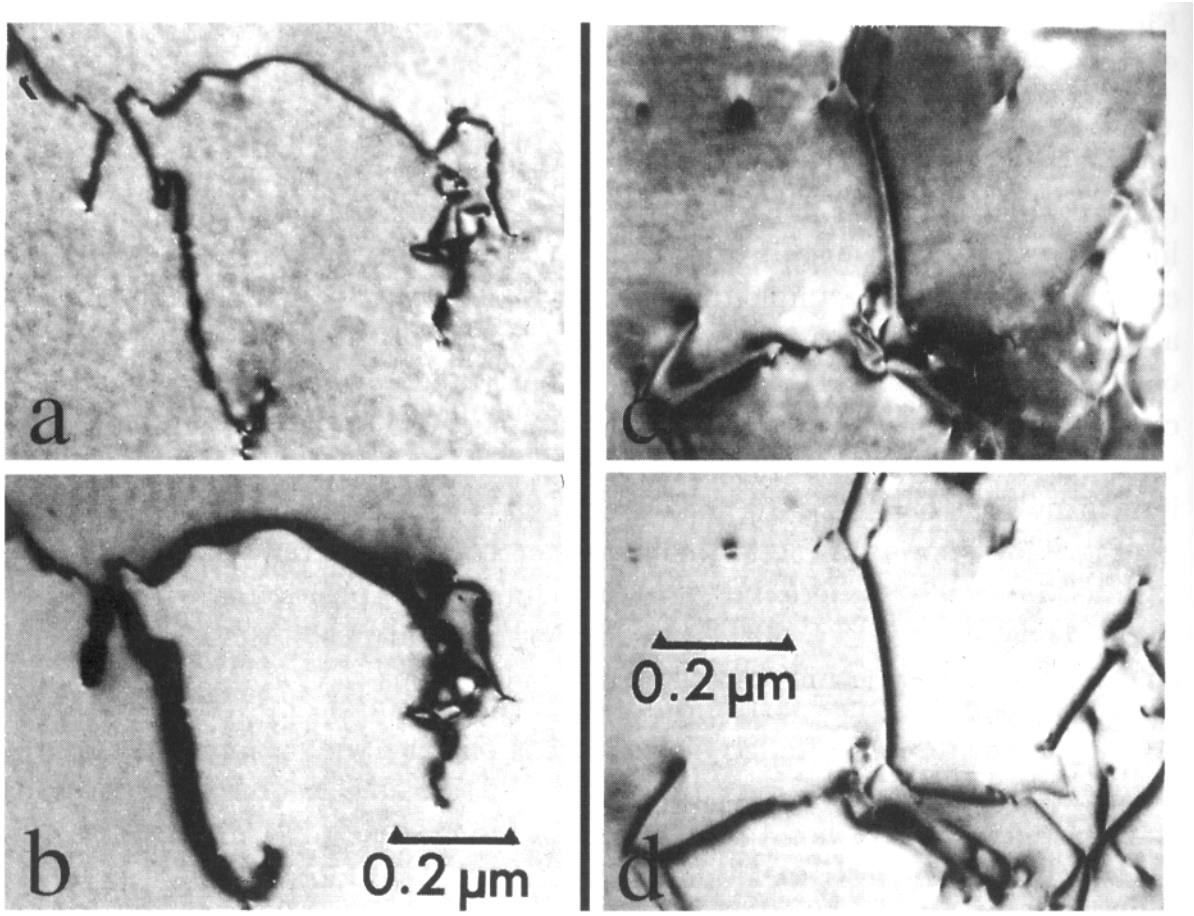

Double image
g*b=2, s=0

Single image
g*b=2,
s is not 0

Fig. 7.33. BF images of dislocations in Al showing: (**a**) single dislocation images in a two-beam BF condition, (**b**) a double image of the same dislocations with two strongly-active diffracted beams, (**c**) a double image for dislocations with $\boldsymbol{g} \cdot \boldsymbol{b} = 2$, $s = 0$, and (**d**) a single image for the same dislocations with $\boldsymbol{g} \cdot \boldsymbol{b} = 2$ and $s \neq 0$. After [7.2].

Example of using g • b = 0 to determine burgers vectors

Copper foil micrographs taken with different 111 type reflections
Burgers vectors of type a/2 [110]

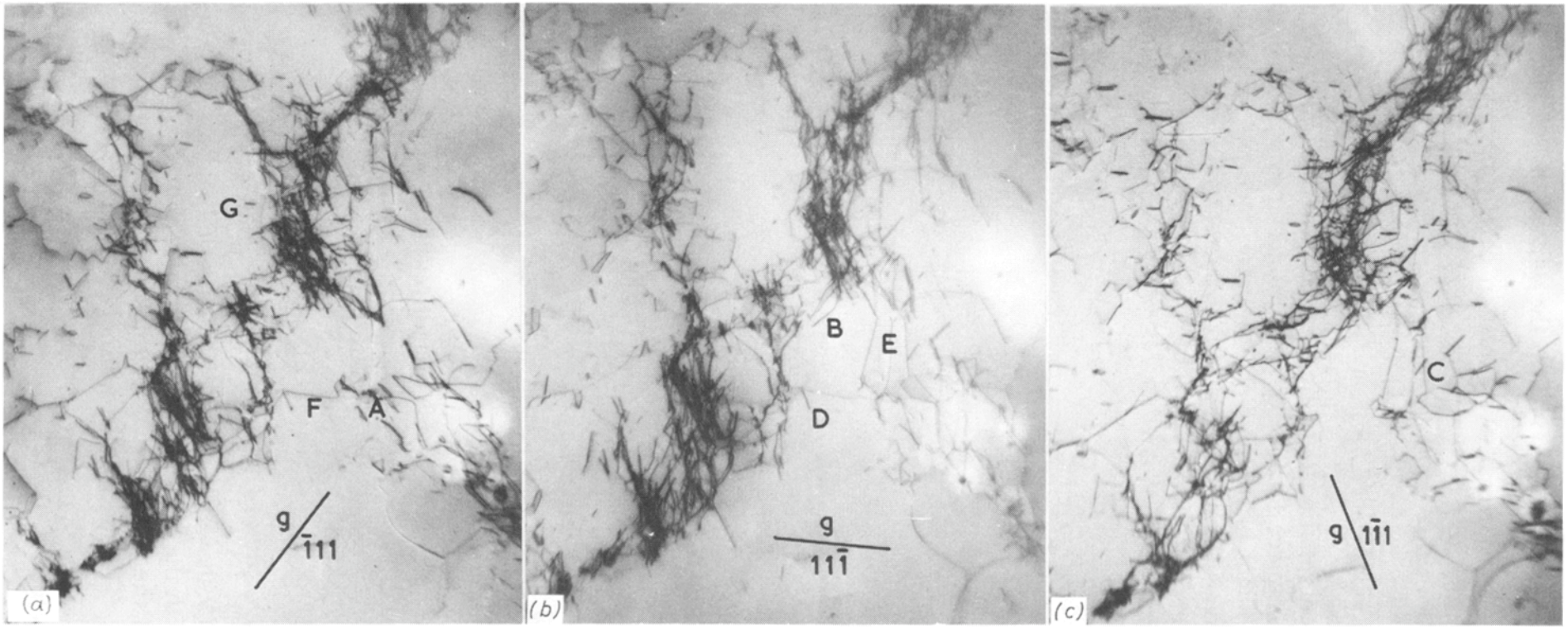

Burgers vectors which *disappear:*		
(a)	(b)	(c)
0-11	-110	-101
101	011	011
110	101	110

Burger's vectors:

A=[011] D=[-101]
B=[110] E=[0-11]
C=[0-11] F=[-101]
G does not disappear
Most likely faulted dipole a/3 [111]

Q: Edge or screw?
A: Mostly edge

Stacking Fault Contrast

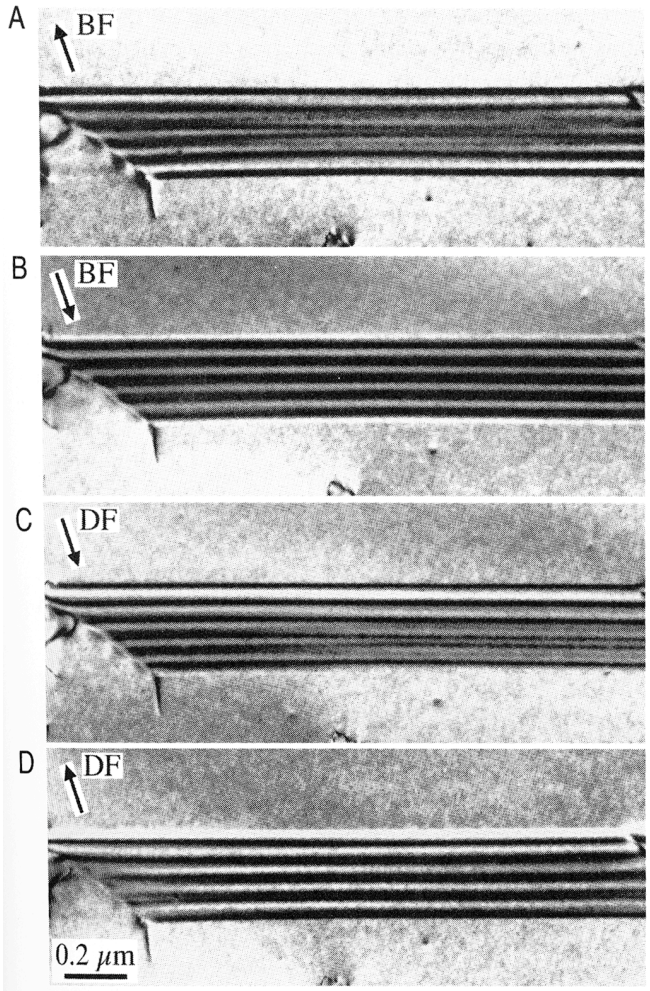

E

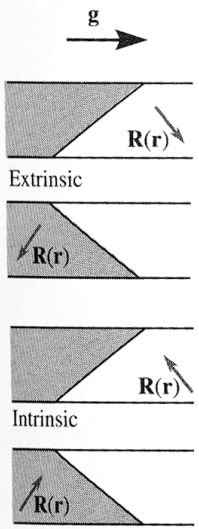

F

	Type A				Type B			
	BF		DF		BF		DF	
B/T	B	T	B	T	B	T	B	T
	G	G	W	G	W	W	G	W
T/B	T	B	T	B	B	B	T	B
	W	W	W	G	G	G	G	W
B/T	B	T	B	T	B	T	B	T
	W	W	G	W	G	G	W	G
T/B	T	B	T	B	T	B	T	B
	G	G	G	W	W	W	W	G

Figure 24.4. (A–D) Four strong-beam images of an SF recorded using ±**g** BF and ±**g** DF. The beam was nearly normal to the surfaces; the SF fringe intensity is similar at the top surface but complementary at the bottom surface. The rules are summarized in (E) and (F) where G and W indicate that the first fringe is gray or white, and (T,B) indicates top/bottom.

Stacking Fault and Interstitial Loop Contrast

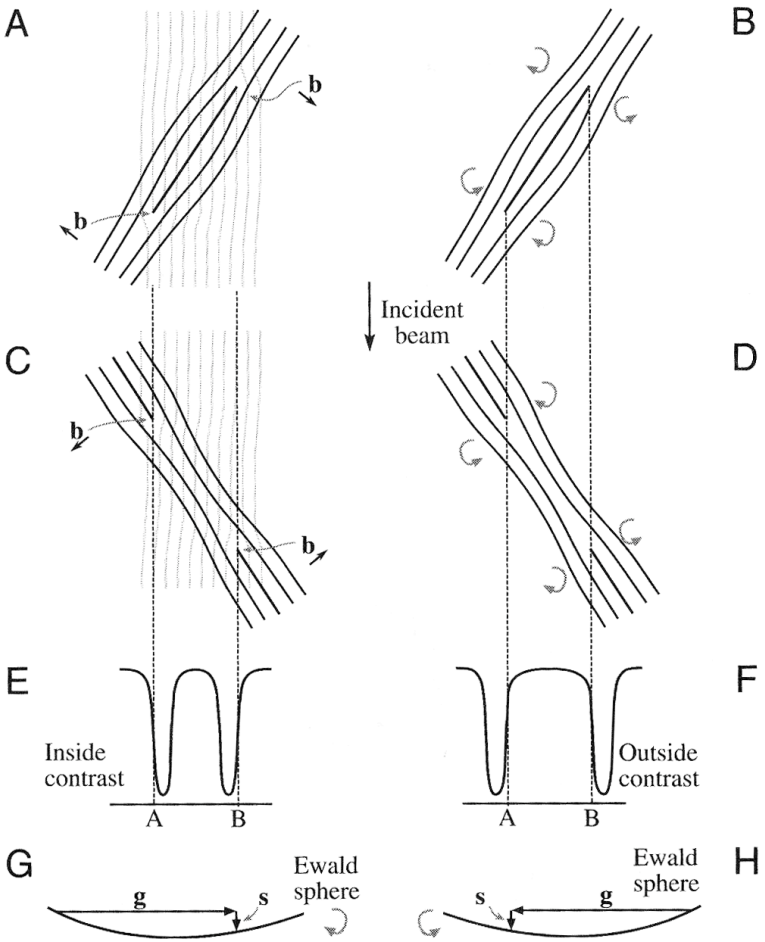

Figure 25.9. (A) Structure of an interstitial loop relative to the diffracting planes (faint lines). (B) Arrows show the rotation of the diffracting planes around the dislocation. (C,D) Vacancy loops. (E,F) Position of the image contrast relative to the projected dislocation position. Inside contrast occurs when clockwise rotation of the diffracting planes brings them into the Bragg condition. Outside contrast occurs for the counterclockwise case. (G,H) The relationship between **g**, **s** and the sense of rotation. Everything is reversed if the loops are tilted in the opposite direction relative to the beam (i.e., reflect this figure in a mirror).

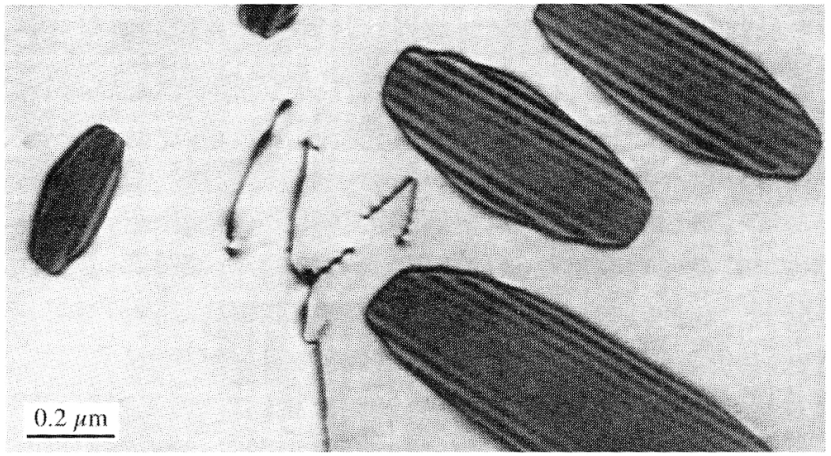

Figure 25.10. Dislocation loops in irradiated Ni showing SF contrast.

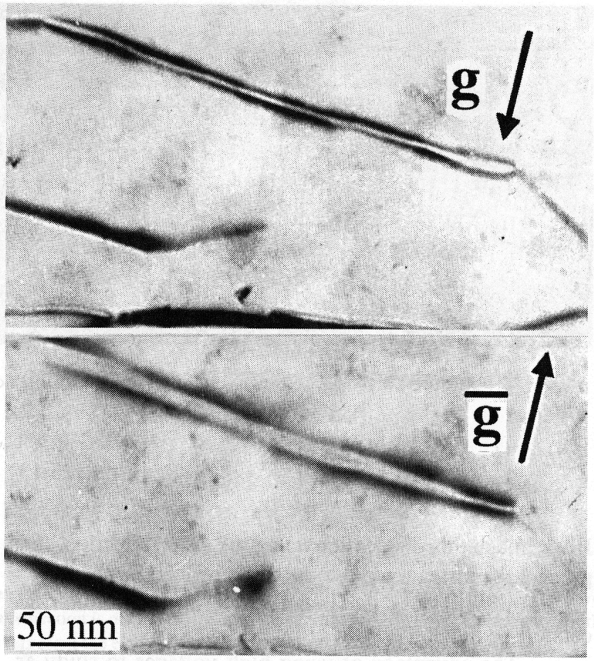

Figure 25.13. Images of dislocation dipoles in Cu showing inside–outside contrast on reversing **g** (±220).

Thin Foil Effects - Thickness Fringes

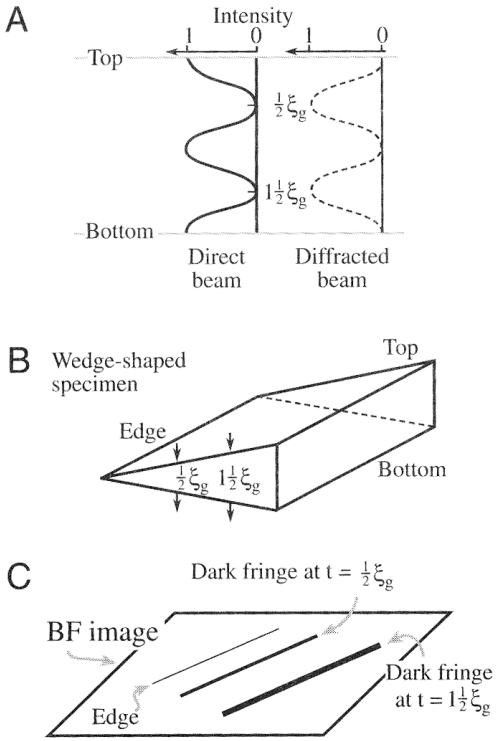

Figure 23.2. (A) At the Bragg condition (s = 0), the intensities of the direct and diffracted beams oscillate in a complementary way. (B) For a wedge specimen, the separation of the fringes in the image (C) is determined by the angle of the wedge and the extinction distance, ξ_g.

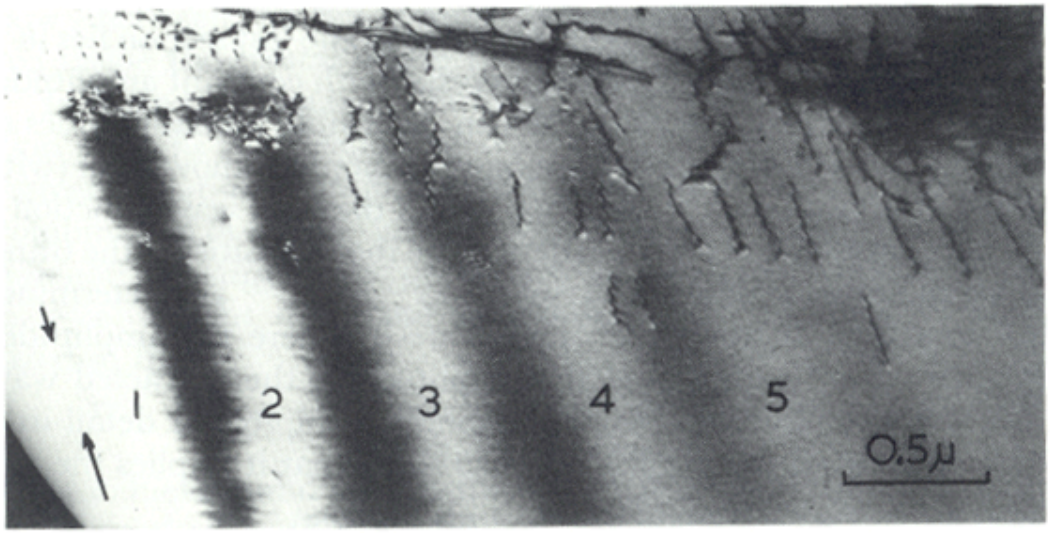

Figure 8.2. Thickness fringes observed in a bright-field micrograph of Cu + 7% Al *alloy. The bright fringes are numbered from the edge of the foil (see arrows). About five fringes are observed. Compare with Figure 8.4c*
(From Hashimoto, Howie and Whelan, 1962, by courtesy of The Royal Society)

Thickness Fringes along Grain Boundaries

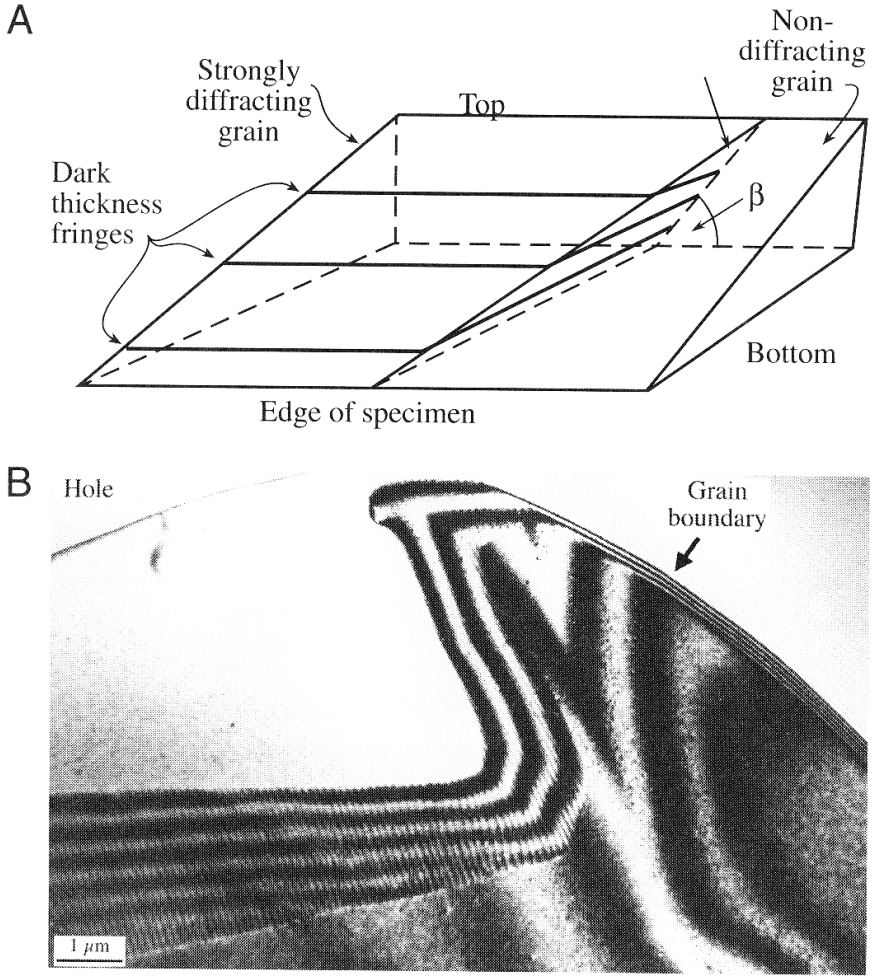

Figure 24.10. (A) If the adjoining grains are rotated so that they do not share a common reflection, images can be formed where only one of the grains diffracts. As shown in (B), the thickness fringes associated with the wedge-shaped foil merge into the thickness fringes associated with the inclined interface. (C) If the foil is tilted so that the same (though not co-incident) reflection is excited in both grains, the number of fringes in the interface increases with each incremental increase in the wedge thickness.

Thin Foil Effects – Bend Contours

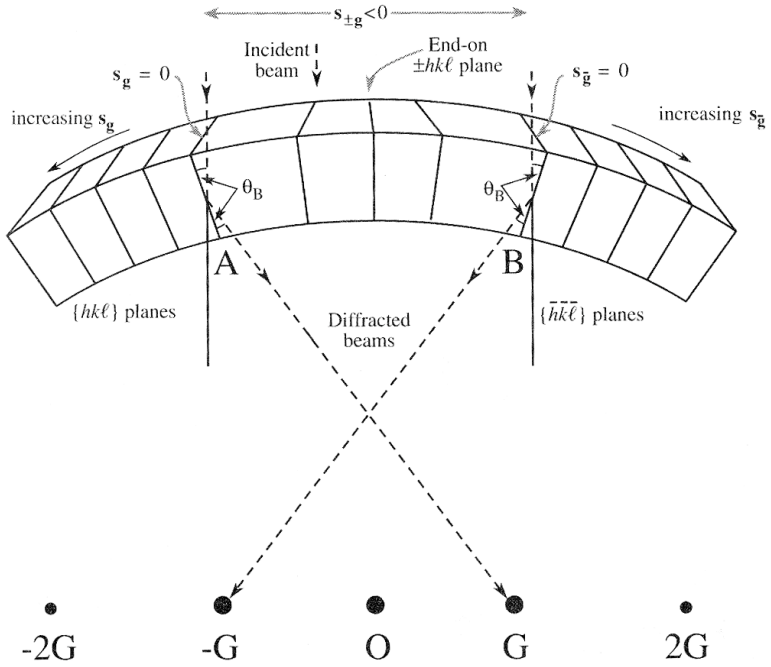

Figure. 23.7. The origin of bend contours shown for a foil symmetrically bent either side of the Bragg conditions. For this geometry, when the $hk\ell$ planes are in the Bragg condition, the reflection G is excited. Notice that G and the diffracting region are on opposite sides of O; if the foil were bent upwards, they would be on the same side.

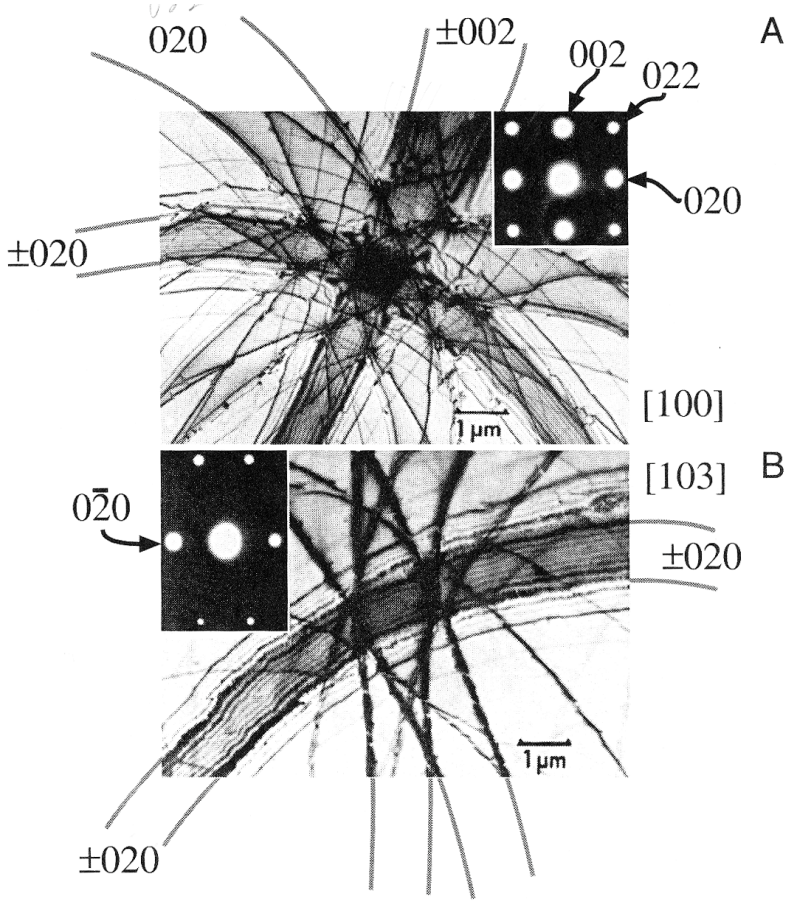

Figure. 23.8. BF images of a bent Al specimen oriented close to the (A) [100] and (B) [103] zone axes. These images are known as (real-space) ZAPs, or zone-axis patterns, and are shown with their respective zone-axis diffraction patterns (insets). Each diffracting plane produces two bend contours, depending on whether θ_B or $-\theta_B$ is satisfied. Note that the separation of the bend contours is not uniform for any particular pair of planes because the curvature of the bending is not, in general, the same.

Thin Foil Effects –
Thickness Fringes and Effect on Stacking Faults

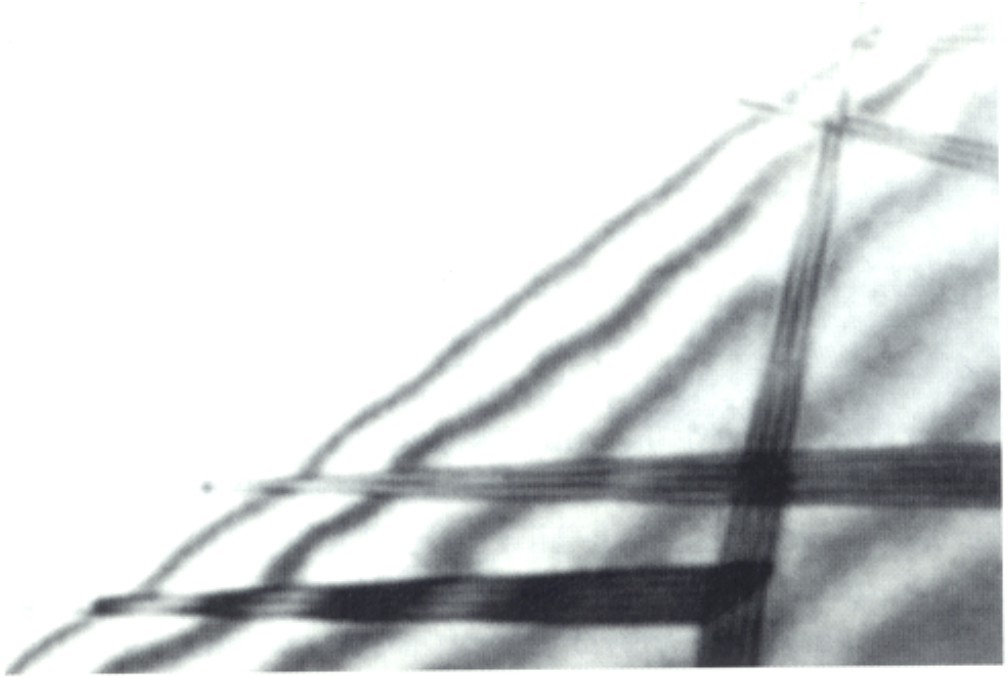

BF image of stacking faults in a wedge-shaped specimen of Ta-C. The four faults appear wedge-shaped, owing to the increasing thickness of the specimen away from the edge.

Thin Foil Effects - Surface Effects on Dislocations

Problems - surfaces

- **Observations performed in thin foils (100 - 200 nm thick), therefore surface forces may be important.**
- **Surface forces may cause glissile dislocations to be lost to the foil surface**
- **The force** (Lothe, in Elastic Strain Fields and Dislocation Mobility, volume 31 Eds. Indenbom and Lothe, 1991) **on a straight dislocation inclined to a free surface is**

$$dF = \frac{1}{\lambda}\left(-E\cot\theta + \frac{\partial E}{\partial \theta}\right)d\lambda$$

Line length **orientation**

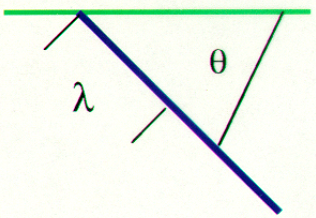

•CONSEQUENCES

•Dislocations will rotate toward the screw orientation as the surface is approached - HREM images

•separation of partial dislocations will be different at the surface than in the bulk.

Thin Foil Effects -
Surface Effects on Dislocations

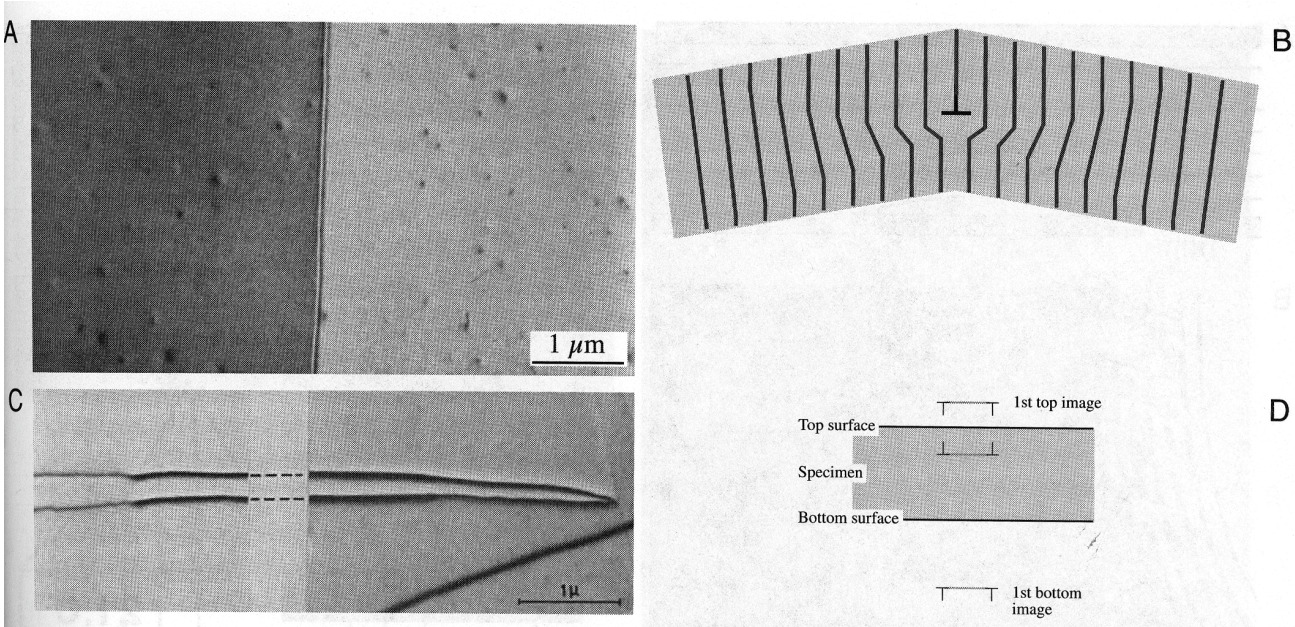

Figure 25.16. (A) A single-edge dislocation lying parallel to the surface of a very thin foil of $SnSe_2$ causes the diffracting planes to bend (B) so we see different intensity in the matrix on either side of the defect. (C,D) If the dislocation is dissociated, the image forces due to the surface cause its width to decrease. The schematic in (D) shows the image dislocations included to represent the effect of the surface.

Thin Foil Effects - Surface Effects on Dislocations

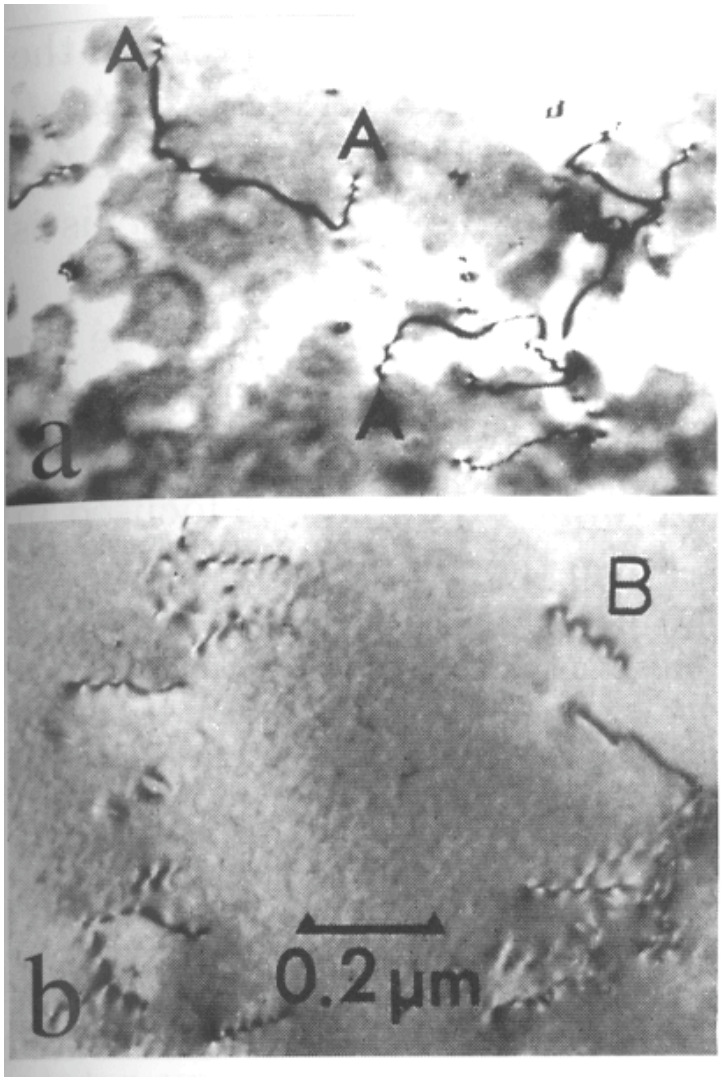

BF images of dislocations in Al showing:

(a) dotted contrast at three locations "A" near the foil surface,

(b) oscillating contrast at the steeply-inclined dislocation "B" due to dynamical effects.

Examples: Grain Boundaries & Dislocations

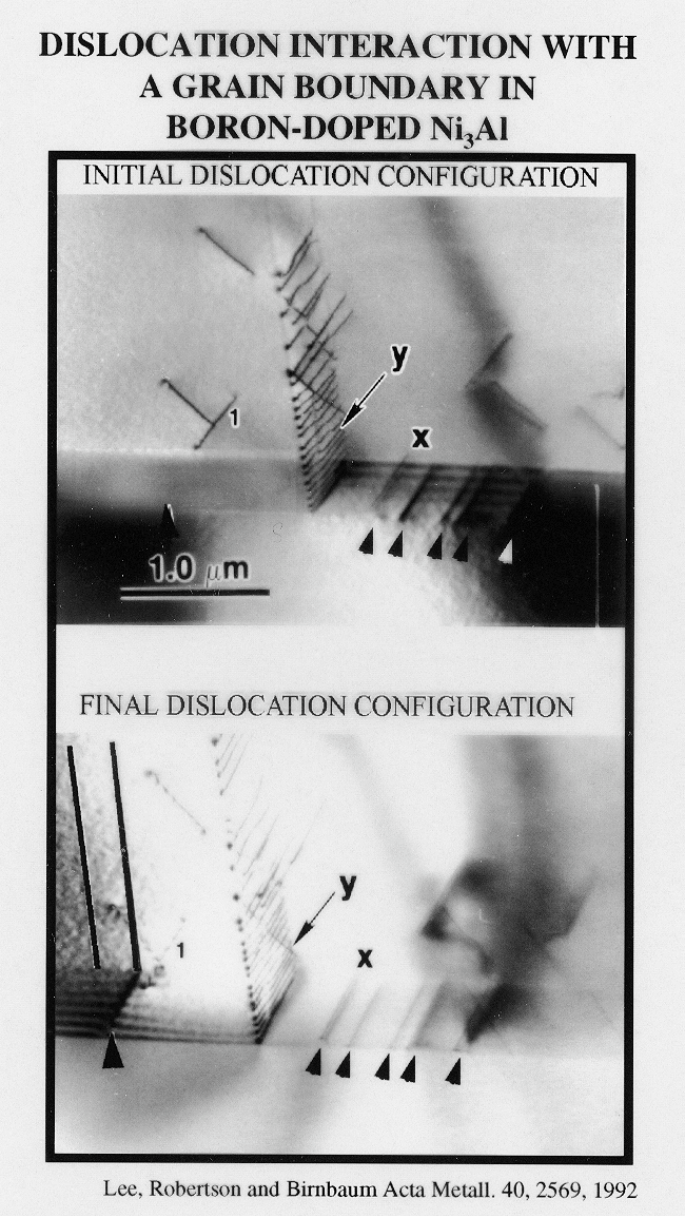

Examples: Dislocations

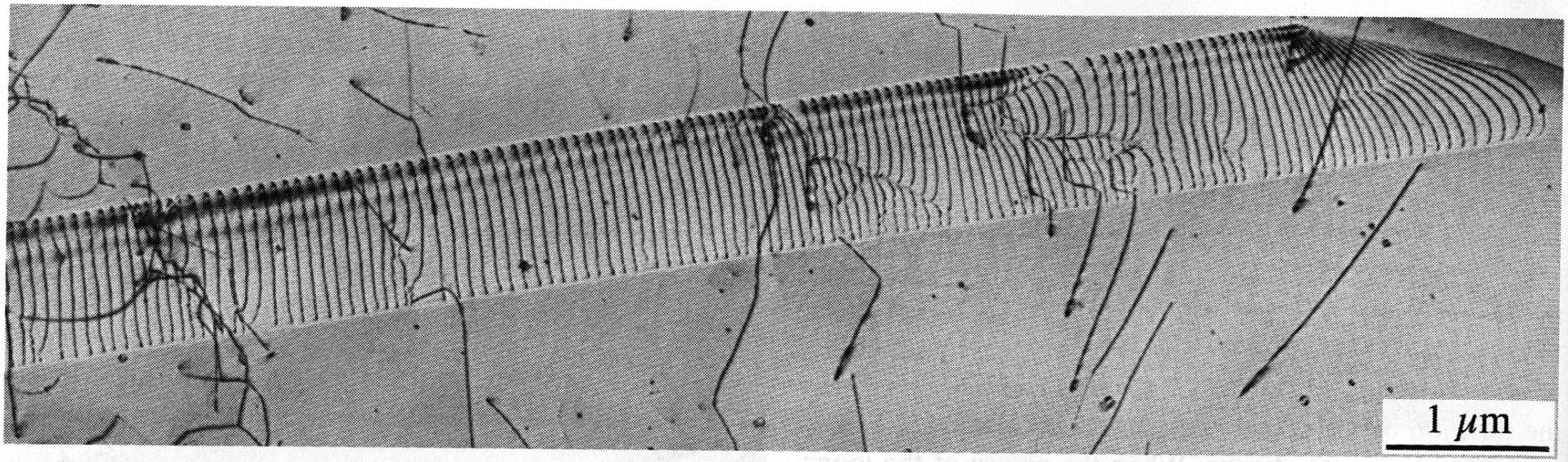

Figure 25.14. Dislocations threading through a very thick specimen in an image recorded using a high-voltage TEM.

Examples: Twins

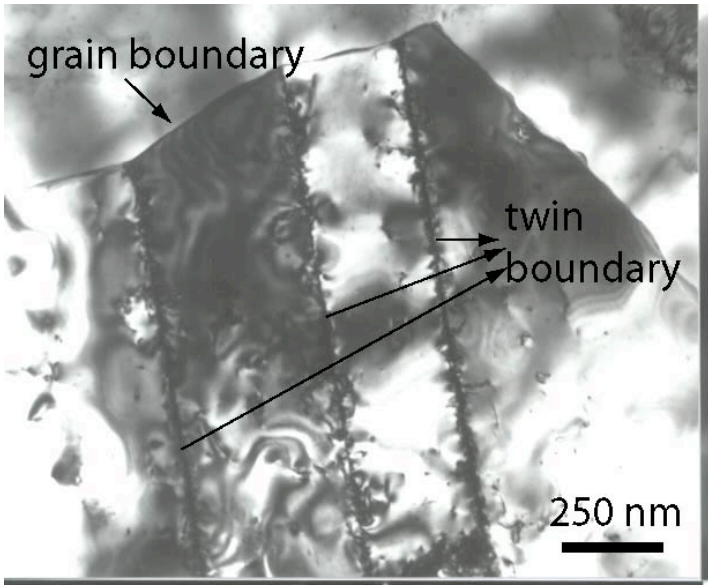

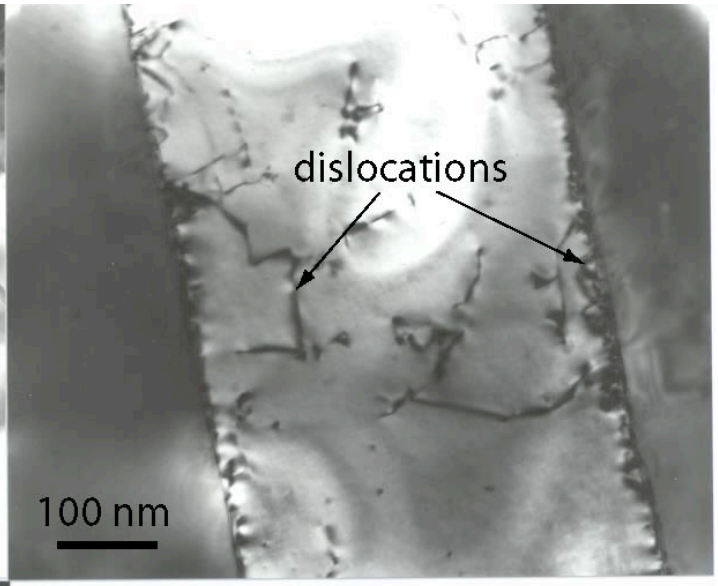

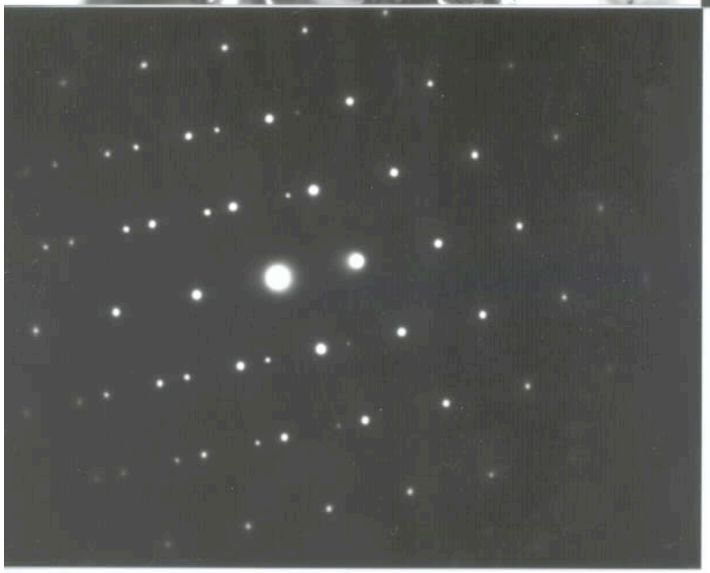

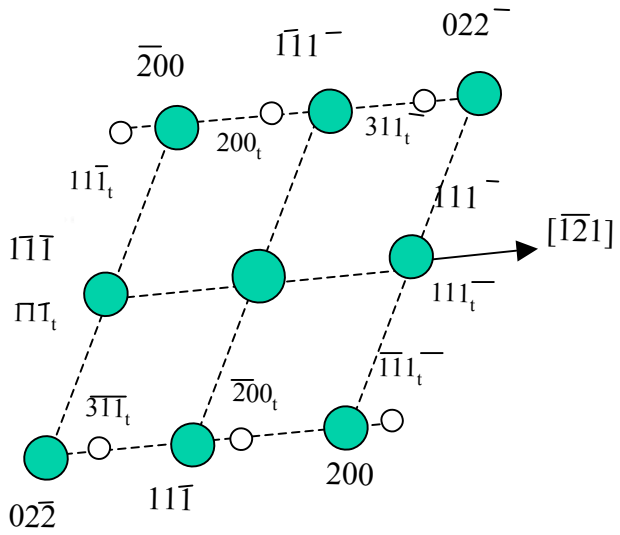

Work done by Dr. Chung-Ming Li

Examples: Twins

WBDF image

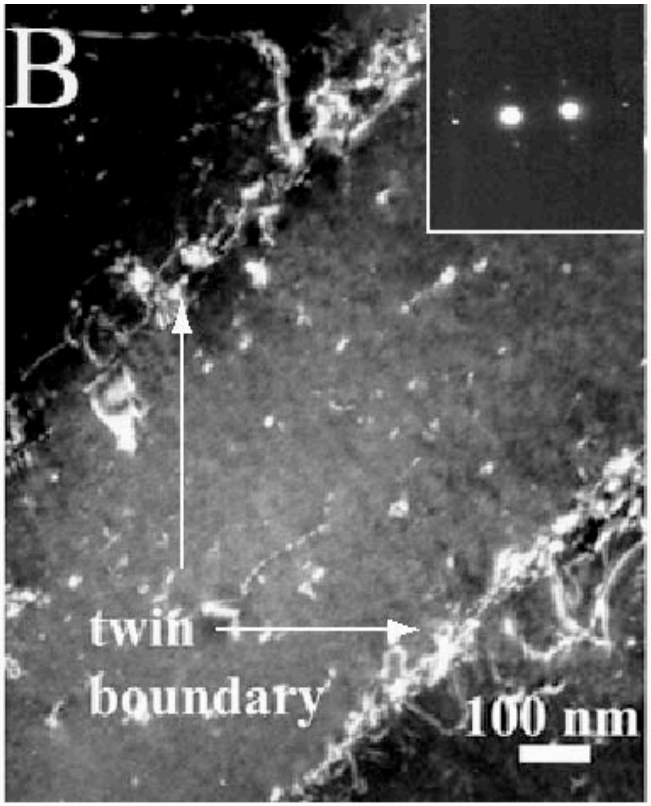

BF image

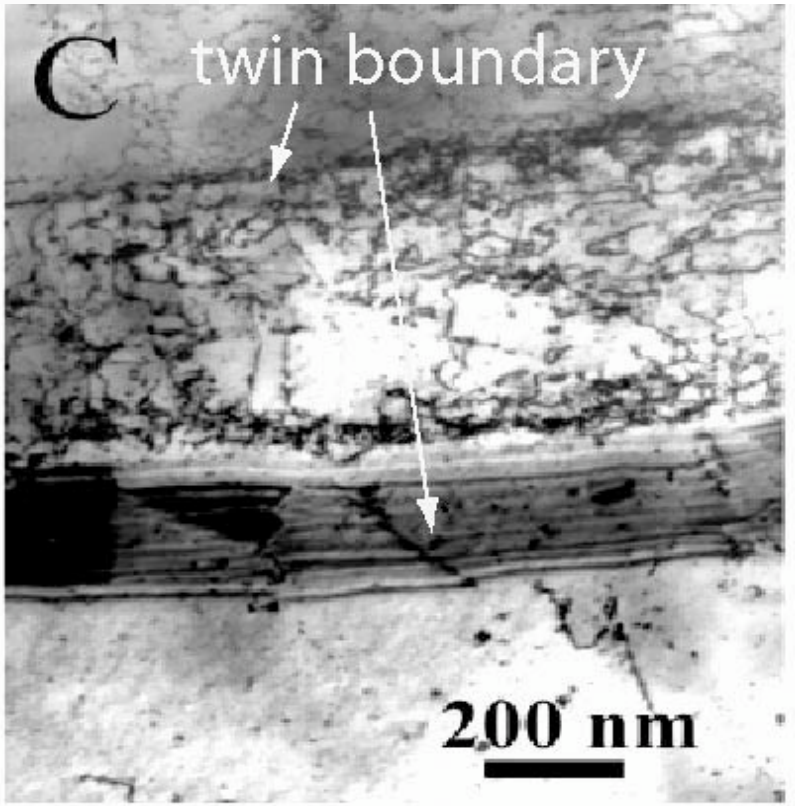

Work done by Dr. Chung-Ming Li

Examples: Twins

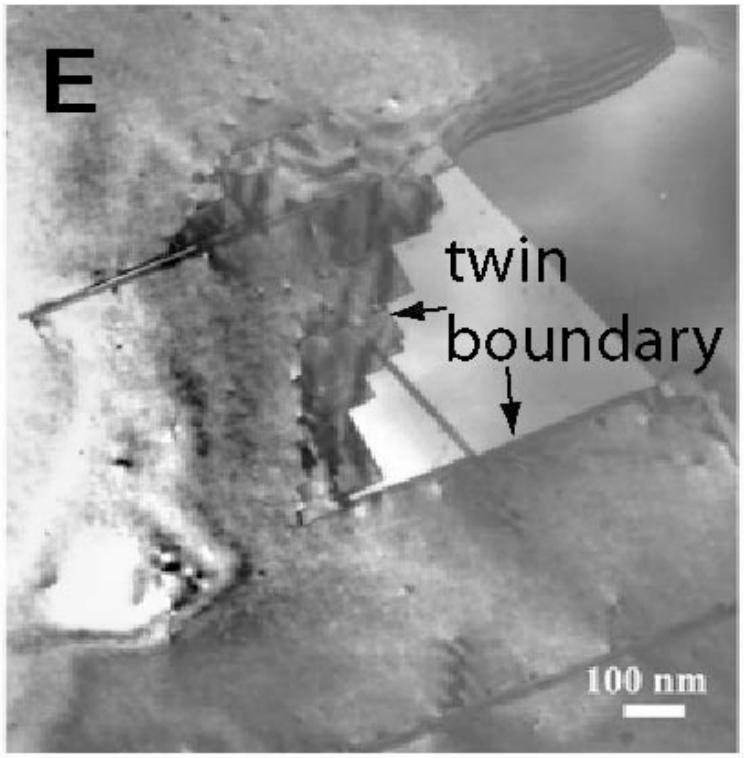

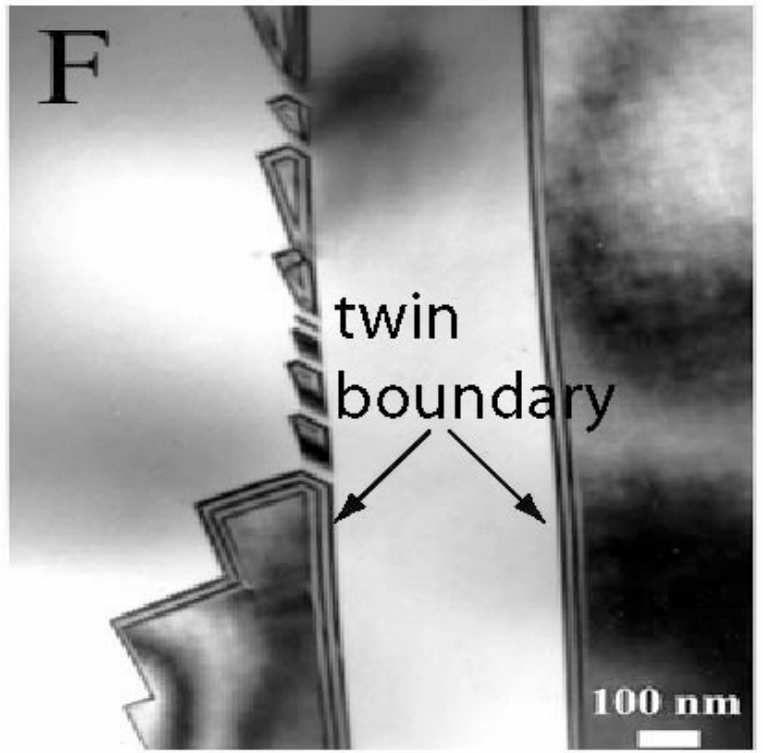

Work done by Dr. Chung-Ming Li

Examples: Movies

Formation and annihilation of stacking faults at twin boundary

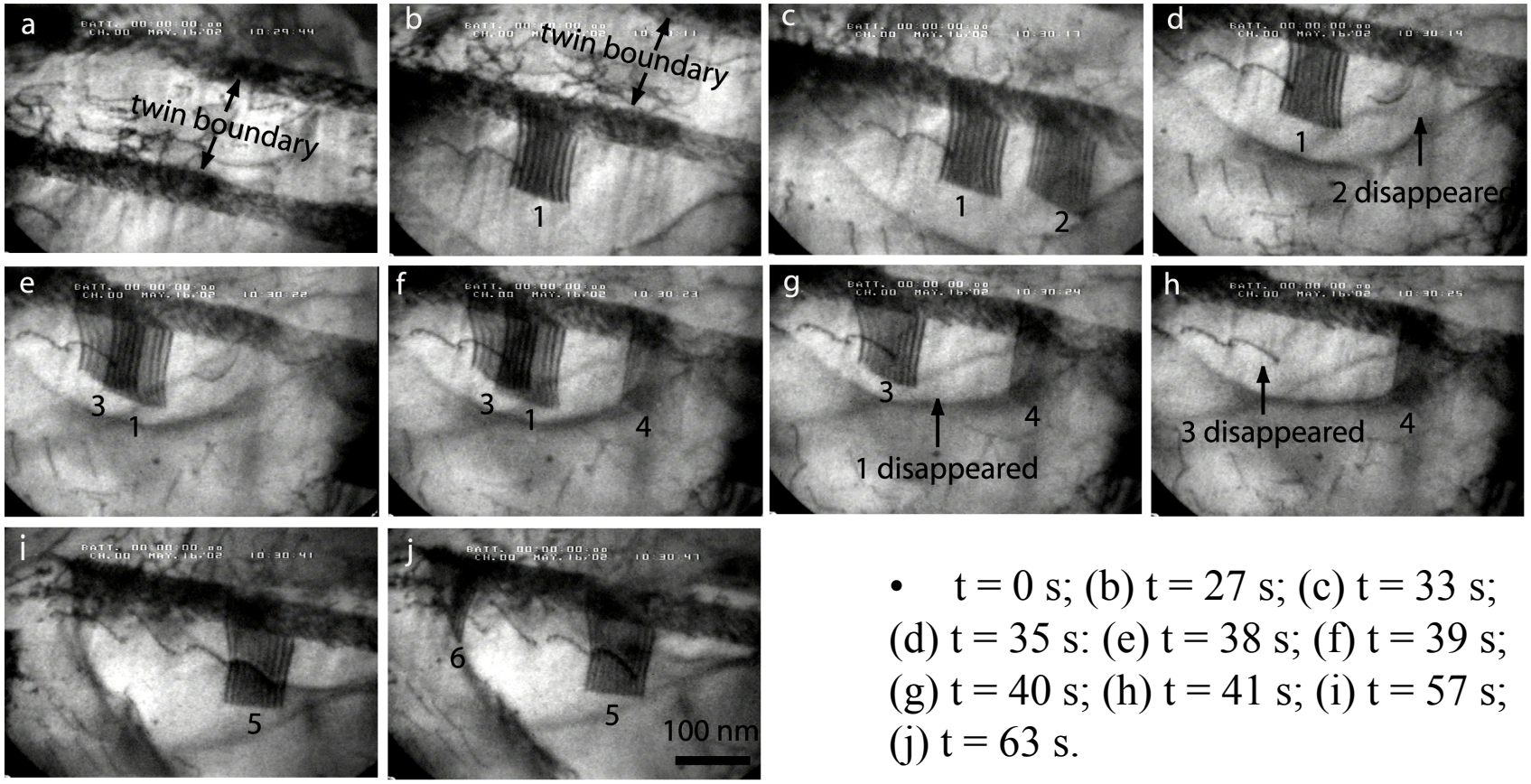

- t = 0 s; (b) t = 27 s; (c) t = 33 s; (d) t = 35 s: (e) t = 38 s; (f) t = 39 s; (g) t = 40 s; (h) t = 41 s; (i) t = 57 s; (j) t = 63 s.

Work done by Dr. Chung-Ming Li